NOAA Technical Memorandum NWS WR-203

AN INVESTIGATION OF THE 24 SEPTEMBER 1986 "COLD SECTOR" TORNADO OUTBREAK IN NORTHERN CALIFORNIA

John P. Monteverdi
Scott A. Braun

Department of Geosciences
San Francisco State University
San Francisco, California
October 1988

U.S. DEPARTMENT OF COMMERCE / National Oceanic and Atmospheric Administration / National Weather Service

NOAA TECHNICAL MEMORANDA
National Weather Service, Western Region Subseries

The National Weather Service (NWS) Western Region (WR) Subseries provides an informal medium for the documentation and quick dissemination of results not appropriate, or not yet ready, for formal publication. The series is used to report on work in progress, to describe technical procedures and practices, or to relate progress to a limited audience. These Technical Memoranda will report on investigations devoted primarily to regional and local problems of interest mainly to personnel, and hence will not be widely distributed.

Papers 1 to 25 are in the former series, ESSA Technical Memoranda, Western Region Technical Memoranda (WRTM); papers 24 to 59 are in the former series, ESSA Technical Memoranda, Weather Bureau Technical Memoranda (WBTM). Beginning with 60, the papers are part of the series, NOAA Technical Memoranda NWS. Out-of-print memoranda are not listed.

Papers 2 to 22, except for 5 (revised edition), are available from the National Weather Service Western Region, Scientific Services Division, P.O. Box 11188, Federal Building, 125 South State Street, Salt Lake City, Utah 84147. Paper 5 (revised edition), and all others beginning with 25 are available from the National Technical Information Service, U.S. Department of Commerce, Sills Building, 5285 Port Royal Road, Springfield, Virginia 22161. Prices vary for all paper copies; microfiche are $3.50. Order by accession number shown in parentheses at end of each entry.

ESSA Technical Memoranda (WRTM)

2 Climatological Precipitation Probabilities. Compiled by Lucianne Miller, December 1965.
3 Western Region Pre- and Post-FP-3 Program, December 1, 1965, to February 20, 1966. Edward D. Diemer, March 1966.
5 Station Descriptions of Local Effects on Synoptic Weather Patterns. Philip Williams, Jr., April 1966 (Revised November 1967, October 1969). (PB-17800)
8 Interpreting the RAREP. Herbert P. Benner, May 1966 (Revised January 1967).
11 Some Electrical Processes in the Atmosphere. J. Latham, June 1966.
17 A Digitalized Summary of Radar Echoes within 100 Miles of Sacramento, California. J. A. Youngberg and L. B. Overaas, December 1966.
21 An Objective Aid for Forecasting the End of East Winds in the Columbia Gorge, July through October. D. John Coparanis, April 1967.
22 Derivation of Radar Horizons in Mountainous Terrain. Roger G. Pappas, April 1967.

ESSA Technical Memoranda, Weather Bureau Technical Memoranda (WBTM)

25 Verification of Operation Probability of Precipitation Forecasts, April 1966-March 1967. W. W. Dickey, October 1967. (PB-176240)
26 A Study of Winds in the Lake Mead Recreation Area. R. P. Augulis, January 1968. (PB-177830)
28 Weather Extremes. R. J. Schmidli, April 1968 (Revised March 1986). (PB86 177672/AS)
29 Small-Scale Analysis and Prediction. Philip Williams, Jr., May 1968. (PB178425)
30 Numerical Weather Prediction and Synoptic Meteorology. CPT Thomas D. Murphy, USAF, May 1968. (AD 673365)
31 Precipitation Detection Probabilities by Salt Lake ARTC Radars. Robert K. Belesky, July 1968. (PB 179084)
32 Probability Forecasting--A Problem Analysis with Reference to the Portland Fire Weather District. Harold S. Ayer, July 1968. (PB 179289)
36 Temperature Trends in Sacramento--Another Heat Island. Anthony D. Lentini, February 1969. (PB 183055)
37 Disposal of Logging Residues Without Damage to Air Quality. Owen P. Cramer, March 1969. (PB 183057)
39 Upper-Air Lows Over Northwestern United States. A.L. Jacobson, April 1969. PB 184296)
40 The Man-Machine Mix in Applied Weather Forecasting in the 1970s. L.W. Snellman, August 1969. (PB 185068)
43 Forecasting Maximum Temperatures at Helena, Montana. David E. Olsen, October 1969. (PB 185762)
44 Estimated Return Periods for Short-Duration Precipitation in Arizona. Paul C. Kangieser, October 1969. (PB 187763)
46 Applications of the Net Radiometer to Short-Range Fog and Stratus Forecasting at Eugene, Oregon. L. Yee and E. Bates, December 1969. (PB 190476)
47 Statistical Analysis as a Flood Routing Tool. Robert J.C. Burnash, December 1969. (PB 188744)
48 Tsunami. Richard P. Augulis, February 1970. (PB 190157)
49 Predicting Precipitation Type. Robert J.C. Burnash and Floyd E. Hug, March 1970. (PB 190962)
50 Statistical Report on Aeroallergens (Pollens and Molds) Fort Huachuca, Arizona, 1969. Wayne S. Johnson, April 1970. (PB 191743)
51 Western Region Sea State and Surf Forecaster's Manual. Gordon C. Shields and Gerald B. Burdwell, July 1970. (PB 193102)
52 Sacramento Weather Radar Climatology. R.G. Pappas and C. M. Veliquette, July 1970. (PB 193347)
54 A Refinement of the Vorticity Field to Delineate Areas of Significant Precipitation. Barry B. Aronovitch, August 1970.
55 Application of the SSARR Model to a Basin without Discharge Record. Vail Schermerhorn and Donal W. Kuehl, August 1970. (PB 194394)
56 Areal Coverage of Precipitation in Northwestern Utah. Philip Williams, Jr., and Werner J. Heck, September 1970. (PB 194389)
57 Preliminary Report on Agricultural Field Burning vs. Atmospheric Visibility in the Willamette Valley of Oregon. Earl M. Bates and David O. Chilcote, September 1970. (PB 194710)
58 Air Pollution by Jet Aircraft at Seattle-Tacoma Airport. Wallace R. Donaldson, October 1970. (COM 71 00017)
59 Application of PE Model Forecast Parameters to Local-Area Forecasting. Leonard W. Snellman, October 1970. (COM 71 00016)
60 An Aid for Forecasting the Minimum Temperature at Medford, Oregon, Arthur W. Fritz, October 1970. (COM 71 00120)
63 700-mb Warm Air Advection as a Forecasting Tool for Montana and Northern Idaho. Norris E. Woerner, February 1971. (COM 71 00349)
64 Wind and Weather Regimes at Great Falls, Montana. Warren B. Price, March 1971.
65 Climate of Sacramento, California. Tony Martini, January 1988. (PB88 206370/AS)
66 A Preliminary Report on Correlation of ARTCC Radar Echoes and Precipitation. Wilbur K. Hall, June 1971. (COM 71 00829)
69 National Weather Service Support to Soaring Activities. Ellis Burton, August 1971. (COM 71 00956)
71 Western Region Synoptic Analysis-Problems and Methods. Philip Williams, Jr., February 1972. (COM 72 10433)
74 Thunderstorms and Hail Days Probabilities in Nevada. Clarence M. Sakamoto, April 1972. (COM 72 10554)
75 A Study of the Low Level Jet Stream of the San Joaquin Valley. Ronald A. Willis and Philip Williams, Jr., May 1972. (COM 72 10707)
76 Monthly Climatological Charts of the Behavior of Fog and Low Stratus at Los Angeles International Airport. Donald M. Gales, July 1972. (COM 72 11140)
77 A Study of Radar Echo Distribution in Arizona During July and August. John E. Hales, Jr., July 1972. (COM 72 11136)
78 Forecasting Precipitation at Bakersfield, California, Using Pressure Gradient Vectors. Earl T. Riddiough, July 1972. (COM 72 11146)
79 Climate of Stockton, California. Robert C. Nelson, July 1972. (COM 72 10920)
80 Estimation of Number of Days Above or Below Selected Temperatures. Clarence M. Sakamoto, October 1972. (COM 72 10021)
81 An Aid for Forecasting Summer Maximum Temperatures at Seattle, Washington. Edgar G. Johnson, November 1972. (COM 73 10150)
82 Flash Flood Forecasting and Warning Program in the Western Region. Philip Williams, Jr., Chester L. Glenn, and Roland L. Raetz, December 1972, (Revised March 1978). (COM 73 10251)
83 A comparison of Manual and Semiautomatic Methods of Digitizing Analog Wind Records. Glenn E. Rasch, March 1973. (COM 73 10669)
86 Conditional Probabilities for Sequences of Wet Days at Phoenix, Arizona. Paul C. Kangieser, June 1973. (COM 73 11264)
87 A Refinement of the Use of K-Values in Forecasting Thunderstorms in Washington and Oregon. Robert Y.G. Lee, June 1973. (COM 73 11276)
89 Objective Forecast Precipitation Over the Western Region of the United States. Julia N. Paegle and Larry P. Kierulff, September 1973. (COM 73 11946/3AS)
91 Arizona "Eddy" Tornadoes. Robert S. Ingram, October 1973. (COM 73 10465)
92 Smoke Management in the Willamette Valley. Earl M. Bates, May 1974. (COM 74 11277/AS)
93 An Operational Evaluation of 500-mb Type Regression Equations. Alexander E. MacDonald, June 1974. (COM 74 11407/AS)
94 Conditional Probability of Visibility Less than One-Half Mile in Radiation Fog at Fresno, California. John D. Thomas, August 1974. (COM 74 11555/AS)
95 Climate of Flagstaff, Arizona. Paul W. Sorenson, and updated by Reginald W. Preston, January 1987. (PB87 143160/AS)
96 Map type Precipitation Probabilities for the Western Region. Glenn E. Rasch and Alexander E. MacDonald, February 1975. (COM 75 10428/AS)
97 Eastern Pacific Cut-Off Low of April 21-28, 1974. William J. Alder and George R. Miller, January 1976. (PB 250 711/AS)
98 Study on a Significant Precipitation Episode in Western United States. Ira S. Brenner, April 1976. (COM 75 10719/AS)
99 A Study of Flash Flood Susceptibility-A Basin in Southern Arizona. Gerald Williams, August 1975. (COM 75 11360/AS)
102 A Set of Rules for Forecasting Temperatures in Napa and Sonoma Counties. Wesley L. Tuft, October 1975. (PB 246 902/AS)
103 Application of the National Weather Service Flash-Flood Program in the Western Region. Gerald Williams, January 1976. (PB 253 053/AS)
104 Objective Aids for Forecasting Minimum Temperatures at Reno, Nevada, During the Summer Months. Christopher D. Hill, January 1976. (PB 252 866/AS)
105 Forecasting the Mono Wind. Charles P. Ruscha, Jr., February 1976. (PB 254 650)
106 Use of MOS Forecast Parameters in Temperature Forecasting. John C. Plankinton, Jr., March 1976. (PB 254 649)
107 Map Types as Aids in Using MOS PoPs in Western United States. Ira S. Brenner, August 1976. (PB 259 594)
108 Other Kinds of Wind Shear. Christopher D. Hill, August 1976. (PB 260 437/AS)
109 Forecasting North Winds in the Upper Sacramento Valley and Adjoining Forests. Christopher E. Fontana, September 1976. (PB 273 677/AS)
110 Cool Inflow as a Weakening Influence on Eastern Pacific Tropical Cyclones. William J. Denney, November 1976. (PB 264 655/AS)
112 The MAN/MOS Program. Alexander E. MacDonald, February 1977. (PB 265 941/AS)
113 Winter Season Minimum Temperature Formula for Bakersfield, California, Using Multiple Regression. Michael J. Oard, February 1977. (PB 273 694/AS)
114 Tropical Cyclone Kathleen. James R. Fors, February 1977. (PB 273 676/AS)
116 A Study of Wind Gusts on Lake Mead. Bradley Colman, April 1977. (PB 268 847)
117 The Relative Frequency of Cumulonimbus Clouds at the Nevada Test Site as a Function of K-Value. R.F. Quiring, April 1977. (PB 272 831)
118 Moisture Distribution Modification by Upward Vertical Motion. Ira S. Brenner, April 1977. (PB 268 740)
119 Relative Frequency of Occurrence of Warm Season Echo Activity as a Function of Stability Indices Computed from the Yucca Flat, Nevada, Rawinsonde. Darryl Randerson, June 1977. (PB 271 290/AS)
121 Climatological Prediction of Cumulonimbus Clouds in the Vicinity of the Yucca Flat Weather Station. R.F. Quiring, June 1977. (PB 271 704/AS)
122 A Method for Transforming Temperature Distribution to Normality. Morris S. Webb, Jr., June 1977. (PB 271 742/AS)
124 Statistical Guidance for Prediction of Eastern North Pacific Tropical Cyclone Motion - Part I. Charles J. Neumann and Preston W. Leftwich, August 1977. (PB 272 661)
125 Statistical Guidance on the Prediction of Eastern North Pacific Tropical Cyclone Motion - Part II. Preston W. Leftwich and Charles J. Neumann, August 1977. (PB 273 155/AS)
126 Climate of San Francisco. E. Jan Null, February 1978. Revised by George T. Pericht, April 1988. (PB88 208624/AS)
127 Development of a Probability Equation for Winter-Type Precipitation Patterns in Great Falls, Montana. Kenneth B. Mielke, February 1978. (PB 281 387/AS)
128 Hand Calculator Program to Compute Parcel Thermal Dynamics. Dan Gudgel, April 1978. (PB 283 080/AS)
129 Fire whirls. David W. Goens, May 1978. (PB 283 866/AS)
130 Flash-Flood Procedure. Ralph C. Hatch and Gerald Williams, May 1978. (PB 286 014/AS)
131 Automated Fire-Weather Forecasts. Mark A. Mollner and David E. Olsen, September 1978. (PB 289 916/AS)
132 Estimates of the Effects of Terrain Blocking on the Los Angeles WSR-74C Weather Radar. R.G. Pappas, R.Y. Lee, B.W. Finke, October 1978. (PB 289767/AS)
133 Spectral Techniques in Ocean Wave Forecasting. John A. Jannuzzi, October 1978. (PB291317/AS)
134 Solar Radiation. John A. Jannuzzi, November 1978. (PB291195/AS)
135 Application of a Spectrum Analyzer in Forecasting Ocean Swell in Scuthern California Coastal Waters. Lawrence P. Kierulff, January 1979. (PB292716/AS)
136 Basic Hydrologic Principles. Thomas L. Dietrich, January 1979. (PB292247/AS)
137 LFM 24-Hour Prediction of Eastern Pacific Cyclones Refined by Satellite Images. John R. Zimmerman and Charles P. Ruscha, Jr., January 1979. (PB294324/AS)
138 A Simple Analysis/Diagnosis System for Real Time Evaluation of Vertical Motion. Scott Heflick and James R. Fors, February 1979. (PB294216/AS)
139 Aids for Forecasting Minimum Temperature in the Wenatchee Frost District. Robert S. Robinson, April 1979. (PB298339/AS)

This publication has been reviewed

and is approved for publication by

Scientific Services Division,

Western Region.

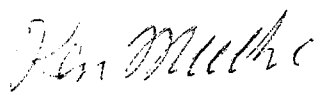

Kenneth B. Mielke, Acting Chief
Scientific Services Division
Western Region Headquarters
Salt Lake City, Utah

TABLE OF CONTENTS

LIST OF TABLES

LIST OF FIGURES

AN INVESTIGATION OF THE 24 SEPTEMBER 1986 "COLD SECTOR" TORNADO OUTBREAK IN NORTHERN CALIFORNIA

ABSTRACT

Several cold-sector tornadoes and funnel clouds were observed in the Sacramento and San Joaquin Valleys of California on 24 September 1986. The synoptic pattern which occurred that day was one long-recognized by operational meteorologists as being associated with severe weather in the state. Mesoanalyses of hourly aviation observations and examination of radar analyses, infrared satellite images, isodrosotherm and surface streamline analyses showed that the tornadoes were associated with a classical right-moving supercell thunderstorm. This cell developed near Redding where warm, moist upvalley flow was experiencing surface convergence ahead of a post-frontal trough. The tornadoes, which formed on a wall-cloud on the southwest portion of the cell, were associated with the occurrence of other features observed with such events in the Great Plains including collapsing radar top, rear flank downdraft and mesolow-mesohigh couplet. The vertical shear profile was also similar to that found with typical supercells including a curved hodograph indicating wind veer with height and vertical speed shear comparable to that observed with supercells in the Great Plains. The air mass over the Central Valley underwent profound destabilization during the day due to differential temperature and moisture advection, low-level diurnal heating and layer-lifting such that stability indices attained values also comparable to those found in regions experiencing approaching risk of severe thunderstorms. As in the Great Plains, dynamic forcing played a significant role in the thunderstorm development. Quasi-geostrophic diagnostics showed that strong upwards vertical motions passed across northern and central California on this day. The vertical motion field was partially associated with a short-wave trough embedded in west-northwest flow which moved across the state and the ageostrophic accelerations produced by a jet-streak which was also advancing across the state. Some simple calculations showed that the vertical motions associated with the jet streak were of the same order of magnitude as those found with the short-wave trough further east. The results of this study underscored the need for forecasters on the West Coast to be familiar with the techniques of operational mesoanalysis of severe weather.

AN INVESTIGATION OF THE 24 SEPTEMBER 1986 "COLD SECTOR" TORNADO OUTBREAK IN NORTHERN CALIFORNIA

I. INTRODUCTION

Tornadoes and severe thunderstorms have historically been considered to be nonsignificant features of the climatology of California. Certainly an examination of climatological statistics seems to bear out the commonly-held notion that tornadoes and severe thunderstorms of the sort observed in the Great Plains rarely, if ever, occur in the state. For example, Court (1974) found that the mean annual tornado incidence varied from 0 to 2 per 26000 km^2 across California for the period 1955-1967 and that an average total of 2 to 3 such storms occurred statewide annually. This should be contrasted with the frequency for most of the southern Great Plains of 12 to 16 per 26000 km^2.

Operational meteorologists know, however, that the relative infrequency of severe weather events in the state certainly does not justify the bias that classic supercell thunderstorms do not occur in California and that the occurrence of such storms should not merely be dismissed as part of the forecasting problem here. It is true that supercell thunderstorms (occurring singly or in clusters) may be infrequently observed in the Western Region. It is also true that when warm season severe weather events occur west of the Rockies, classic strong to severe thunderstorms are often the cause (see, for e.g., Fontana, 1977; Lussky, 1986; and, Randerson, 1986).

In addition, preconceived notions that tornadoes are not only an infrequently observed but also an absent phenomenon in the state may someday have serious repercussions. This attitude, alluded to by Bluestein (1979), is not supported by the evidence. In fact, Hales (1985) reported that tornado frequencies in the Los Angeles Basin are comparable to those observed in portions of the central United States. Furthermore, an evaluation of recent tornado statistics suggests that the past estimates of tornado frequency in California do not reflect current trends in the data. Hales (1985), using data for the period 1962-1983, reported a mean tornado incidence of 4 to 5 per year for the state. The authors have analyzed records from the National Severe Storms Forecast Center (NSSFC) for the period 1950-1986 and have found similar frequencies. Most of this slight increase has occurred in the years following the early 1970's and it is not clear whether it is due to an actual increase in numbers of tornadoes, greater numbers of people present to observe them or more awareness on the part of the public that such storms can be a hazard in the state. In any case, it is certainly true that despite the relative low frequency of tornadoes in California, significant damage and several injuries have been attributed to them.

The authors realize that many operational meteorologists in the portions of the Western Region most likely to experience severe weather events are already aware of the forecasting problems associated with them. Indeed, several studies on cold sector tornadoes and funnel clouds by Western Region personnel will be alluded to below. However, since there is a perception that severe thunderstorms are not a SYSTEMATIC feature of the climate of the Western Region in general, California in particular, the authors felt that a study of one particularly spectacular outbreak of tornadic thunderstorms would do much to dispel the myth that classic tornadic supercells do not occur here. The storm in question developed in the northern Sacramento Valley on 24 September 1986 and was associated with three verified tornadoes, including an F2, several funnel clouds and large hail. The parent thunderstorm developed in an environment which was remarkably similar to that which is present when tornadic dry-line supercells occur in the Great Plains. We believe that this storm is more than the subject of an interesting case

study and that its development underscores the need for all operational meteorologists in the Western Region to be thoroughly acquainted with the mesodynamics of severe weather.

II. COLD SECTOR TORNADOES IN CALIFORNIA

Tornadoes in California most often form in the cold, conditionally unstable air mass behind a cold front (Fawbush and Miller, 1954; Hales, 1985) and, as a result, are referred to as cold sector tornadoes. Cold sector tornadoes tend to form in an area of scattered showers and isolated thundershowers (Lacy, 1968) where convective cloud patterns in the area of development may show considerable enhancement and may organize into a nonfrontal comma cloud (Monteverdi, 1976; Reed, 1979; Mullen, 1979; Reed and Blier, 1986). Since such storms develop in a cool air mass characterized by relatively low mixing ratios, potential instability is less of a factor in the development of such storms than in the formation of those observed commonly in the Great Plains (Monteverdi et al., 1988). Because of this, standard stability indices such as the Lifted Index (LI), the K-index and the Showalter Index may not indicate the potential for severe weather (Halvorson, 1971; Cooley, 1978).

Once formed, cold sector tornadoes are generally weak in nature (F0 or F1 intensity) and are characterized by a slender, ropelike appearance, a short and narrow path, and a very short lifespan (Fawbush and Miller, 1954). Such funnels and tornadoes have been documented in California by Fawbush and Miller (1954), Halvorson (1971), Smith (1971), Hales (1985) and Monteverdi et al. (1988). Cold sector tornadoes have also been observed in England (Lacy, 1968), in Michigan (Cooley, 1978), in Washington state (Holmes, 1982) and Utah (NOAA, 1984a).

Tornadoes in California occur most often with wave cyclones of the "high latitude type", as defined by Weaver (1962). These storms are associated with very cold, conditionally unstable air masses moving southeastward from the Gulf of Alaska (Weaver, 1962) and often develop on the western side of an amplifying longwave trough (Reed and Blier, 1986). Smith (1971) and Reed and Blier (1986) have suggested that the southeastward movement of the storm systems over gradually warmer ocean or land surfaces destablizes the air masses further so that convection becomes more likely later in the life cycle of these disturbances. The air masses may also destabilize under the influence of strong cold advection at jet stream levels over California. Besides providing a favorable thermodynamic environment, these high latitude type storms are generally associated with upper tropospheric divergence diagnosed by moderate to strong midtropospheric cyclonic vorticity advection (Reed and Blier, 1986) and vertical motions induced by upper tropospheric jet streaks (Hales, 1985; Reed and Blier, 1986; Monteverdi et al., 1988) located over or northwest of the state. The relationship of cloud features to 300 mb trough axis and jet streak in such situations is well-illustrated by Figure 1. This schematic diagram depicts the locations of such features on March 21, 1987 when funnel clouds and large hail occurred in the San Joaquin Valley (Monteverdi et al., 1988).

Although most California tornadoes are weak, strong tornadoes (F2) are not uncommon and several severe (F3) tornadoes have been observed in the state (Figure 2). Smith (1971) estimated the upper limit for tangential wind speeds for California tornadoes to be 175 miles per hour (mph) with a translational speed of 15 to 25 mph. Data for the period 1950-1986 indicated that the mean path length for tornadoes in the state is 0.92 miles and the mean path area is 0.06 square miles.

Tornado formation in California appears to be strongly influenced by topographic features. Locations of all tornado occurrences in California for the period 1950-1986 were plotted (not shown) according to latitude and longitude coordinates. The resulting pattern revealed two major regions prone to tornado formation: i. in northern and central California from the gap in the coastal range near San Francisco to the Central Valley and encompassing the portion of the valley from Red Bluff to just south of Fresno; and, ii. in southern California from Burbank south to San Diego and eastward to the western edge of the Mojave desert. These results are in general agreement with the findings of Hales (1985) with only a slight modification of the tornado prone areas. The high tornado frequency in the Central Valley may be due partially to stronger diurnal heating effects there, convergence of flow through the coastal range near San Francisco, and/or topographically induced confluence when southerly flow impinges northwards through the Sacramento Valley (Weaver, 1962; Hales, 1985; and, Monteverdi et al., 1988). Hales (1985) suspected that the high frequency in the Los Angeles area may be the result of frictional convergence caused by the juxtaposition of the coastline and the mountains in southern California.

III. OVERVIEW OF THE CENTRAL VALLEY TORNADO OUTBREAK OF 24 SEPTEMBER 1986

A. Visual Observations

At approximately 1730 UTC (0930 LST) 24 September 1986, surface observations and radar reports (discussed below) indicated that a thunderstorm was developing rapidly west of Redding, California (N.B.: all locations shown in Figure 3 with location identifiers listed in Table 1). The storm was forming in the relatively unstable air mass (discussed below) which had flowed into Northern California following the passage of a surface cold front at around 1000 UTC (0200 LST). Between 1915 and 1945 UTC (1115-1145 LST), a funnel cloud either reached the ground or got close enough to the ground to damage several structures in Cottonwood (located between Redding and Chico).

Table 1: Location identifiers for stations reporting hourly observations used in mesoanalyses.

ACV	Arcata	SAC	Sacramento
BIH	Bishop	SCK	Stockton
CEC	Crescent City	SFO	San Francisco Int'l
CIC	Chico	SJC	San Jose Int'l
FAT	Fresno Air Terminal	STS	Santa Rosa
MOD	Modesto	SUU	Travis Air Force Base
MYV	Marysville	SVE	Susanville
OAK	Oakland Int'l Airport	TRK	Truckee
RDD	Redding	TVL	Tahoe Valley Airport
RNO	Reno	UKI	Ukiah

At approximately 2015 UTC (1215 LST), a tornado, rated an F2 by the NSSFC (U.S.D.C., 1986), was spotted near Vina, just north of Chico. Pictures of this tornado, taken from Highway 99 looking west, are shown in Figures 4a-c. These photos were taken within a 15 minute period. Note that there were at least two funnel clouds decending from the wall cloud and that, at one time, two of the funnels were in contact with the ground. The brighter area in the left part of the pictures suggests that a rear flank downdraft may have been present.

Between 2000-2200 UTC (1300-1400 LST), funnel clouds continued to be spotted as the main thunderstorm mass moved south-southeastward. Chico police reported that the funnel cloud touched down again just east of Chico (Fontana, 1986).

At 2358 UTC (1558 LST) 24 September, personnel at the National Weather Service Office (WSO) at Stockton reported a funnel. This report was erroneously transmitted as a pilot report at 0015 UTC 25 September (1615 LST 24 September). Then, 9 minutes later a pilot reported that a funnel was just touching the ground southeast of Stockton. Both reports are shown below:

NMCPIRCA
UBUS90 KWBC 250015
SCK UUA /OV SCK /TM 2355 /FLOG /RM FUNNEL CLD APRXM 10 E ARPT

NMCPIRCA
UBUS90 KWBC 250024
SCK UUA /OV LIN130015 /TM 0012 /FL UKN /TP C180 /RM FUNNEL
CLD 15 SE LIN JUST TOUCHING GROUND

There were no reports of further funnel clouds or tornadoes following the 0024 UTC (1624 LST) pilot report. Thunderstorms continued affecting the area for several hours, however.

B. Synoptic Overview

A facsimile of the NMC surface map for 1800 UTC (1000 LST), a time slightly before the thunderstorm began to develop near Redding, is shown in Figure 5. At this time, the surface cold front was moving through central California and was well south of Redding. This front extended northeastward across the Great Basin into Idaho where it was no longer analyzed.

The 1200 UTC (0400 LST) AVN 500 mb height (decameters) and absolute vorticity ($X\ 10^{-5}$ sec^{-1}) analysis is given in Figure 6. Operational forecasters will recognize this pattern as one which favors severe weather in the Central Valley of California. A strong negatively-tilted short wave trough was located along the British Columbia-Washington coastline. Cyclonic vorticity advection was occurring over the northern half of California. A split in the 500 mb flow was found just north of the San Francisco Bay Area. North of the split westerly winds were characteristic in the mid-troposphere while west-northwesterly flow was typical over north-central California.

The 1801 UTC (1001 LST) infrared satellite image (Figure 7) shows that the frontal band spiraled as an occlusion from Idaho into the surface low west of British Columbia. The portion of this cloud band adjacent to the Washington coastline was a comma-cloud and was analyzed as a polar trough on the surface map. Enhancement of the cloudiness over southeastern Oregon through northwestern California suggests that another trough line may have been located in that area. This point will be corroborated by the mesoanalyses discusssed below.

IV. SURFACE CONTROLS ON THE REDDING STORM

A. Storm Genesis

As expected, mesoanalyses of hourly surface data provided greater insight to the contributing factors in the development of this storm than did the synoptic chart given in Figure 5. The 1900 UTC (1100 LST) mesoanalysis is given in Figure 8a. A most important difference between Figures 5 and 8a is the mesoanalyzed post-frontal trough, the axis of which extends from just east of San Francisco through the northern Sacramento Valley. This feature was responsible for the lack of the pronounced wind veer to northwesterly which usually accompanies a frontal passage in California. Note that all the stations in the Sacramento Valley were reporting upvalley (southerly) winds at this time and that the isodrosotherm analysis shows that air with high dew points was being advected northward through the valley.

At 1840 UTC (1040 LST) a moderate thunderstorm had commenced at Redding (observation not shown). At that time, the gust front from the developing thunderstorm (shown as a dashed, double-dotted line with barbs on figure 8a) had passed the station as winds veered from SSE to SSW with gusts to 30 knots and temperatures fell 5°F from the previous observation.. The mesoanalysis for this time shows that the developing thunderstorm was associated with a mesolow-mesohigh couplet comparable to similar features observed with supercell thunderstorms in the Great Plains (see, for e.g., Doswell, 1986).

Plan position indicator (PPI) displays from the Sacramento National Weather Service radar (WSR-57) are provided in Figures 8b-c. These two radar analyses were for times roughly one-half hour before and after, respectively, the time of the mesoanalysis given in Figure 8a. Note the orientation of the cells roughly paralleling the trough line as they moved eastward. Of special interest is the cell near Redding in Figure 8b. During the one hour interval between Figure 8b and 8c, the video integrator processor (VIP) derived precipitation intensity for this cell increased from level 3 (moderate) to 5 (intense). Note also that the precipitation echo top (40 000 feet) had overshot the tropopause, which was near the 275 mb level (36 000 feet). Some damage occurred at ground level roughly at this time.

Surface streamline analyses were completed using standard isogonal analysis procedures as described by Petterssen (1956, pp. 23-25) and Riehl (1954, pp. 188-192). Figure 8d is the surface streamline analysis for 1900 UTC (1100 LST) 24 September 1986 which roughly corresponded to the time of explosive thunderstorm growth near Redding. The strong confluence evident in the southerly flow in the Valley was obviously an important contributor to the development of the thunderstorms in the north. In this case, topographically-induced confluence in the southerly flow was probably augmented by the confluence into the pressure trough evident in Figure 8a. In addition, since wind speeds were generally uniform over the entire region, with no strong compensating surface velocity divergence evident, the confluent patterns indicated on Figure 8d were approximating surface convergence patterns. Accordingly, one would expect convection to have been favored in the region extending from Stockton on the south to Redding on the north.

Furthermore, such southerly flow undergoes lifting in its passage northward. Weaver (1962) and Hales (1985) have suggested that such topographic effects can destabilize the northward moving flow and can contribute to moisture and temperature advection northward. In particular, Weaver (1962) cited this as a reason why the northern Sacramento Valley is often a

focus for intense convection in much the same way that the Caprock formation in the Texas Panhandle is a preferred location for supercell development (Doswell, 1985). In any case, it is clear that the developing thunderstorm was being fed by warm, moist air entering the right rear (southwestern) side of the storm.

The hemispheric infrared satellite image for 1801 UTC (1001 LST) (roughly an hour before the time of Figure 8a and one-half hour before Figure 8b) is given in Figure 8e and shows the developing cells along the trough line. The developing Redding storm can be seen just east of the two distinct cumulonimbus anvils located over the coastal mountains west of Redding.

B. Tornado Genesis

Tornadoes touched ground with the Redding storm between 1915 and 2015 UTC (1115 and 1215 LST). Figure 9a is the surface mesoanalysis for 2000 UTC (1200 LST), Figure 9b the radar analysis for 2027 UTC (1227 LST), and Figure 9c the surface streamline analysis for 2000 UTC (1200 LST).

The mesolow-mesohigh couplet evident on Figure 8a had moved southeastward and was responsible for a strong backing of the wind at Chico from 1900 UTC (1100 LST) to 2000 UTC (1200 LST) (Figure 9a). Air with relatively high dew point continued to flow northward through the San Joaquin and Sacramento Valleys towards the developing thunderstorm. Figure 9b shows that the mesolow was located roughly near the southwestern periphery of the VIP level 5 precipitation echo associated with the Redding thunderstorm which had moved almost due southeastward. Hodograph analyses (discussed in a later section) show that the storm was moving at an approximate angle of 40^{0} to the right of the mid and upper tropospheric flow and that the storm-relative wind profile favored "ventilation" typical for supercell thunderstorms (Doswell, 1985). A comparision of Figure 9b with Figure 8c shows that top of the storm had collapsed 3000 feet between 1900 and 2000 UTC (1100 and 1200 LST).

It is interesting to note that the development of this cell matched closely the three stages in supercell growth described by Lemon and Doswell (1979). During the first stage, the typical storm turns to the right of the flow and the top of the cell rises substantially. Mid and upper tropospheric winds over the northern Sacramento Valley (discussed in Sections III.B and VII.B.ii) were basically westerly for the entire event. It is clear that the supercell which developed near Redding moved southeastward (to the right of the mean mid to upper tropospheric wind) while it was in the process of building to the upper troposphere.

In the second stage, the updraft continues to intensify and funnel clouds are often observed, a few of which might touch down as weak tornadoes. As discussed above, some ground level damage occurred about the time of Figure 8c, when the storm's top pushed through the tropopause.

The third stage, called the collapse stage, is characterized by increasing radar reflectivity and decreasing updraft intensity. Lowering of the storm's radar reflectivity top (as well as the visual cloud top) often occurs. It is at this stage that the most intense tornadoes occur. They are usually positioned in the zone of strong vertical velocity gradient between the updraft and rear flank downdraft (RFD). The RFD is a secondary downdraft which develops upwind (in this case, westsouthwest) of the updraft and is considered to be of critical importance to tornado formation (Lemon and Doswell, 1979). The tornado tends to develop on the updraft side of the

velocity gradient (on the upwind side of the mesolow) (Lemon and Doswell, 1979; Davies-Jones, 1986).

Photographs often show that the tornado forms beneath the right or rear portion of the wall cloud and also reveal a "clear slot" to the rear or right rear of the tornado. This clear slot is indicative of the existence of a relatively dry RFD (Lemon and Doswell, 1979; Davies-Jones, 1986).

Figure 9b indicates that the overshooting top had collapsed by 2027 UTC (1227 LST). This radar analysis is roughly simultaneous with Figures 4a-c, which showed the F2 tornado which developed near Vina. It is important to note the correspondence between the rear flank clear slot, indicative of the RFD, seen in Figures 4a-c and the collapse of the storm's top, shown in Figure 9b.

The 2000 UTC (1200 LST) streamline analysis (Figure 9c) shows that the northern portion of the valley was no longer receiving an influx of air from the south. Strong confluence continued in the region from around Sacramento to Chico ahead of the trough line which had moved eastward from its previous position. Other strong to severe thunderstorms were developing at this time in the eastern, foothill areas of the Sacramento Valley near Marysville in the moist air moving northward through the valley. At Redding, winds remained southerly as a new weak surface trough began affecting that portion of the state and as outflow from the thunderstorm complex to the south continued.

The 2100 UTC (1300 LST) mesoanalysis is given in Figure 10a. This corresponds roughly to just after the time of tornado touchdown near Chico. The mesolow-mesohigh couplet seen in Figure 9a had shifted southeastward to near Chico. Note that a windshift from southeasterly to westsouthwesterly had occurred at Chico as the mesolow moved east of the city. In addition, dewpoints had dropped from the 50's^{o} F to the middle 40's^{o} F at Redding. This phenomenon probably was associated with both the import of dry rain-cooled midtropospheric air by the RFD and the influx of air with relatively low mixing ratios from the north Pacific behind the first trough line. The trough seen in the previous mesoanalysis had shifted southeastward with windshifts to west-southwesterly characteristic along the coast and a second trough line was located just to the north and west of Redding.

Figures 10b and 10d are the radar analysis and enhanced infrared satellite image for 2130 UTC (1330 LST). The three cells to the east and the one cell to the northwest of Marysville visible on the previous radar analysis had developed into two distinct linearly-organized storms by 2130 UTC (1330 LST) (Figure 10b) but the thunderstorm which produced the Vina tornado was slowly decreasing in intensity. Nevertheless, the tornadic cell was the one most clearly discernible on the satellite image (Figure 10d) with an anvil stretching northeastward into Nevada.

Winds in the Valley to the south of Chico continued to be southerly and to be characterized by high dew points (Figures 10a). In addition, the streamlines (Figure 10c) show that the air with the highest dew points was feeding the right flank of the storm which would insure that it would continue to move to the right of the mean wind aloft.

It is interesting to note that there was approximately a 13^{o}F difference in surface dewpoint temperatures from Modesto to Redding at this time. This corresponded to a difference of 4 g/kg

in mixing ratios across that same area. By 0000 UTC (1600 LST) (shown below) the dewpoint difference had increased to 17°F from Sacramento to Redding which corresponded to a difference in mixing ratios of around 5 g/kg. Most of this gradient was concentrated in the 50 miles or so in the vicinity of the main thunderstorm mass which, at that time, was located near Marysville. Although such a gradient is comparable to that reported by Doswell (1982) as occuring across severe thunderstorms of the "dryline" type in the southern Great Plains, the dryline in this case was not a precursor feature. Ninomaiya (1971) has found that "dryline-like" features can occur after severe thunderstorms have formed when the RFD has developed. The surge of cool, dry air may actually act to intensify the parent storm.

C. New Developments on Right Rear Flank

Figure 11a is the mesoanalysis for 2200 UTC (1400 LST), Figure 11b the radar analysis for 2230 UTC (1430 LST), Figure 11c the streamline analysis for 2200 UTC (1400 LST) and Figure 11d the enhanced infrared imagery for 2230 UTC (1430 LST). Missing observations for Chico, Truckee and Susanville (and, in subsequent mesoanalyses, Oakland, Marysville and Bishop) made it impossible to follow the evolution of the mesolow-mesohigh couplet discussed in previous sections. Nevertheless, the continued progression southeastward of both post-frontal troughs is evident in Figure 11a. Most, though not all, of the radar echoes (Figure 11b) were still found east of the first trough axis with the original supercell found just northeast of Marysville. It is interesting to note that the thunderstorm occuring at Marysville was apparently related to a new development on the southwestern flank of the original tornadic storm (Figure 11d). Most of the active developments were occurring in the confluence of the moist flow east of the axis of the valley (Figures 11a and 11c). Note also the strong confluence north of Modesto and Stockton (Figure 11c) near the cluster of VIP level 4 and 5 echoes evident in that area on Figure 11b.

D. New Tornadogenesis near Stockton

The surface mesoanalyses for 2300 and 0000 UTC (1500 and 1600 LST) are given in Figures 12a and 13a, the radar analyses for 2330 and 0030 UTC (1530 and 1630 LST) are given in Figures 12b and 13b, the surface streamline analyses for 2300 and 0000 UTC (1500 and 1600 LST) are given in Figures 12c and 13c, and the analyzed and hemispheric infrared satellite images for 0000 UTC (1600 LST) are given in Figures 12d and 13d.

While the trough lines continued to move eastward, the main focus for new development shifted southeastward through the valley where strong confluence of air with relatively high dew points continued (Figures 12a, 13a, 12c, and 13c). At 2330 UTC (1530 LST), the convective activity was concentrated in a linearly organized cluster of thunderstorms (Figure 12b) which had apparently formed on the southwestern flank of the main storm mass (Figure 12d). The radar top of the southern-most cell was 34 000 feet (Figure 12b). At 0030 UTC (1630 LST) (Figure 13b), roughly six minutes after the pilot report of a tornado near Stockton, the line had moved southeastward and the elevation of the southern cell's radar top had decreased to 30 000 feet. Again it appears that the tornado formed during the collapse of the storm's radar top. Anvils from the northernmost storms had joined to form a comma-shaped convective cluster which extended from just northeast of Marysville through northwestern Nevada and into northeastern California with the original Redding storm near the tail of the comma (Figures 12d and 13d). It appears that the tornado near Stockton developed on the southwestern portion of a secondary cluster which had formed south and west of the original storm complex.

V. THERMODYNAMIC SETTING

Diurnal changes in the thermodynamic structure of the air mass over northern and central California were of great importance in the development of the thunderstorms during the afternoon of the 24th and contributed to the growth of the severe storms. Several of the mechanisms associated with this destabilization were similar to mechanisms identified in the literature as important in severe thunderstorm growth in the Great Plains (Uccellini and Johnson, 1979; Bluestein and Thomas, 1984; Barnes and Newton, 1986).

Figure 14 shows the 1200 UTC (0400 LST) 24 September Oakland sounding. Nearly saturated air can be found from the surface up to the 720 mb level with a very dry layer above. The superadiabatic lapse rate which characterized the layer from about 740 mb to 695 mb was probably due to "wet bulbing" (a phenomenon which occurs as a wet thermistor leaves a layer characterized by clouds and precipitation) and should not be considered a feature typical of the environment.

This sounding is similar to the typical Oklahoma tornado sounding (Carlson et al., 1983) which features a moist layer near the ground and an elevated dry mixed layer aloft. However, the lifted index (LI) of +2 suggested that the lower atmosphere was relatively stable and that unless destabilization occurred during the day a very low probability of thunderstorms should be expected. However, it should be pointed out that this "stable" LI is somewhat misleading since the sounding was convectively unstable, as discussed below.

Operational forecasters know that the Oakland sounding should not be considered completely representative of the thermodynamic structure in the Sacramento Valley, particularly in the lowest layers. Diurnal heating and cooling effects are stronger in the Central Valley than along the coast (Weaver, 1962). In addition, air masses which cross the coastline and enter the Valley are subject to destabilization as these northward flowing air masses are forced by topography to converge and rise (Weaver, 1962; Hales, 1985).

An examination of Figure 3 shows that the distance between the 1000 foot contours roughly halves from the mouth of the Sacramento Valley to the portion of the Valley near Chico. If northward-moving air columns conserved their three-dimensional volume such that horizonal convergence in their surface layers would be exactly compensated by vertical motions, the depth of each layer would be doubled as the air columns moved from Sacramento to Chico. With these assumptions, an air mass entering the mouth of the Sacramento Valley near Sacramento would, in its lowest layers, be vertically-stretched by a factor of 2 by the time it attained the latitude of Chico. Further stretching would occur as the air streamed into the narrower northern portion of the Valley. Assuming that most of these effects would be restricted to the lowest 2 km (the extent to which southerly flow characterized the Oakland hodograph as discussed below), lifting of the lower layers by around 150 mb would take place.

Analysis of the morning Oakland sounding showed that a layer lifting of only 100 mb would have resulted in a lowering of the LI to -3.5. A lift of an additional 50 mb would have lowered the LI to -5.5. These destabilizations would be in addition to those which might have occurred because of differential temperature advection and diurnal effects.

An examination of Figure 15, the 0000 UTC 25 September (1600 LST 24 September) Oakland sounding, reveals some marked changes in the stability of the atmosphere at that location. The

difference in temperature between 0400 LST and 0000 LST for each layer from the surface to 300 mb (Figure 16) reveals that substantial cooling occurred in the 900 mb to 350 mb layer and that even more profound warming characterized the layer from 940 mb to the surface. This destabilization was accompanied by a decrease in the lifted index from +2 in the morning to -2 in the afternoon. From the surface to about 950 mb, a superadiabatic lapse rate prevailed resulting in a level of free convection at the ground and an equilibrium level at approximately 460 mb.

Examination of mid and upper tropospheric temperature (not shown) and wind patterns (shown below) and low level wind fields (Figures 8d, 9-13c) qualitatively showed that mid and upper tropospheric cold advection as well as diurnal heating were responsible for the temperature changes and destabilization at Oakland suggested by Figure 16. Similar examination suggested that low level warm advection and topographic lifting in the upvalley flow and more significant diurnal heating probably contributed to greater destabilization there. As an estimate of the degree to which the additional effects active in the Central Valley could modify the Oakland sounding, the NSSFC (courtesy Mr. Jack Hales, Lead Forecaster) kindly provided the authors with estimates of the LI in the vicinity of the thunderstorms obtained by substitution of hourly surface aviation temperature and dewpoint information from Valley stations for Oakland's surface data (see Hales and Doswell, 1982 for details). This procedure yielded an LI of about -4 in the storm genesis area. This value is indicative of moderate to high instability and is associated with at least an approaching risk of severe thunderstorms (NOAA, 1984b).

VI. HODOGRAPH ANALYSIS

Barnes and Newton (1986) and Browning (1986) (and many others) have described the importance of strong vertical shear in the generation of severe convection. In general, in an unstable environment a wind strongly veering and increasing in speed with height favors the development of long-lived supercell thunderstorms. This type of wind distribution insures that the warm updraft will not be overwhelmed by precipitation-cooled downdraft air, which is shunted downstream. There is also considerable evidence (see e.g., Lemon and Doswell, 1979) that such a shear profile creates strong relative vorticity around a horizontal axis which is then tilted in the vertical in the updraft. Lemon and Doswell (1979) and Davies-Jones (1986) have shown that the vorticity around a vertical axis which is thus created is of the same order of magnitude seen in tornadoes. They concluded that a wind shear profile characterized by strong directional (veer) and speed shear (increasing winds with height) are prerequisites for tornadic supercell development.

Figure 17 shows (a) the typical wind hodograph for supercell thunderstorms in Alberta (after Chisholm and Renick, 1972) and (b) the 1200 UTC (0400 LST) 24 September 1986 wind hodograph for Oakland, CA. Note that the Oakland hodograph shows a wind veer with elevation similar in aspect to that seen in the typical hodograph. In addition, the vertical speed shear is comparable in both hodographs. The most obvious difference between the two is the strong northwesterly component apparent in the winds aloft at Oakland. Note also that the mean storm motion lay considerably to the right of the mean environmental wind in both cases.

Marwitz (1972) computed stability and wind shear parameters for various types of severe thunderstorms. Table 2 gives (a) these parameters averaged for many supercell cases and (b) the same parameters computed from the 1200 UTC (0400 LST) Oakland sounding. Since, as explained above, the Oakland sounding was not totally representative of the storm environment, we have inserted the LI for Vina (estimate obtained from the NSSFC, see section V above), and

have assumed that the cloud base was located at the lifting condesation level of 970 mb (approximate elevation 300 m).

Table 2. Thermodynamic Stability and Wind Shear Parameters for Well-documented Supercell Storms (after Marwitz, 1972) and for the 24 September 1986 Tornadic Supercell in California (from Oakland sounding)

LI (^{0}C)	Veering in Subcloud Layer (deg)	Mean Subcloud Wind (deg/m s^{-1})	Mean Wind Sfc-10 km (deg/m^{s-1})	Storm Motion (deg/m s^{-1})	Cloud Layer Shear (10^{-3}s^{-1})
Typical Supercells (average values)					
-6.2	68	184/12.8	244/21.8	282/11.4	3.5
Modified Oakland Sounding (see text)					
-4.0	70	178/2.6	299/23.2	330/7.7	4.7

A comparison of the parameters shows the degree to which the shear environment for the Redding storm was similar to that for typical supercells. Note that the LI, wind veer in the subcloud layer and the motion of the storm relative to the mean wind were comparable. Cloud layer shear values were also similar with the greater value at Oakland reflecting the active polar jet stream present in this case. Mean subcloud wind speeds were considerably less for this case than for the typical supercell storm but would have been more comparable if low level winds in the Sacramento Valley, which averaged near 15 knots (7.8 m s^{-1}), had been substituted for the Oakland subcloud layer winds.

Figure 18 is a schematic which depicts the component of the relative windflow acting along the Redding storm's motion. This storm-relative flow (SRF) profile was obtained by subtraction of the mean storm motion vector from the environmental wind at each level shown and by obtaining only the component of the relative flow acting **along** the storm motion. It is clear that the storm motion acted to enhance the low level inflow of moisture laden air from the south and to shunt precipitation-cooled air away from the updraft.

Figure 18 is deceptive because it implies that the storm motion lay on the hodograph. As Doswell (1985) points out, this only occurs if the shear is unidirectional and only due to changes in speed. In reality, the hodograph showed some curvature (Figure 17) and actual SRF vectors (as shown in dashed arrow on figure 17b) were oriented in such a manner that the southwestern flank of the Redding storm had preferential access to warm moist air and that the SRF aloft shunted rain-cooled air east-southeastward out of the path of the storm. As a result, this storm had the characteristics of a classic right-moving supercell.

VII. DYNAMIC FORCING MECHANISMS

When many aspects of a synoptic and mesoscale pattern seem to favor the occurrence of a significant weather event, such as a severe thunderstorm, it is common for operational meteorologists to search for a "trigger" for the activity. This trigger is usually some dynamic

forcing mechanism which creates enough lifting to stimulate either a general outbreak of severe weather or which, together with other factors, helps to focus such activity in a more limited geographic area. For example, one such commonly-known trigger is upper tropospheric divergence, generally diagnosed by cyclonic vorticity advection (CVA) in the middle troposphere. Many studies have shown, however, that consideration of CVA patterns alone can yield a deceptive, and often erroneous, assessment of dynamically-forced vertical motion patterns (see, for e.g., Barnes, 1985).

Quasi-geostrophic diagnostics may be employed to assess more accurately some of the dynamically-forced vertical motions due to ageostrophic circulations in the upper troposphere. For example, the quasi-geostrophic omega equation can be used to estimate the mid-tropospheric vertical motions which arise only because of the local and horizontal advective changes of the geostrophic wind (Bluestein, 1986). Many studies have shown the usefulness of this approach (see, for e.g., Heflick and Fors, 1979; Barnes, 1985; Barnes, 1986; Barnes, 1987; Doswell, 1987; Durran and Snellman, 1987).

However, where intense jet streaks occur in the upper troposphere, terms involving the local and advective changes of the ageostrophic wind become significant in producing vertical motions. Quasi-geostrophic theory quantitatively fails in these cases although the diagnosed patterns may be qualitatively correct if parcel trajectories are not excessively curved (Bluestein, 1986). The possible relationship of jet streak dynamics to the production of severe thunderstorms in the present case study will be discussed below.

A. Quasi-geostrophic Effects

The omega equation is often used to diagnose fields of quasi-geostrophically-forced vertical motions in the middle troposphere. The reader is referred to Holton (1979, pp. 119-143) and Bluestein (1986) for a thorough overview of the nature of quasi-geostrophic theory. For the purposes of this paper, a very simplified solution to the omega equation was used. The omega equation may be written as:

$$(\nabla^2 + f_o^2/\sigma\, \partial^2/\partial p^2)\omega = f_o/\sigma\, \partial/\partial p\left[\mathbf{V_g} \cdot \nabla\left(1/f_o\, \nabla^2\Phi + f\right)\right] + 1/\sigma\, \nabla^2\left[\mathbf{V_g} \cdot \nabla\left(-\partial\Phi/\partial p\right)\right] \quad (1)$$

where ω is the vertical velocity in pressure coordinates, p is pressure, f is the coriolis parameter, σ is the static stability parameter, $\mathbf{V_g}$ is the geostrophic wind, Φ is the geopotential height and $\left(1/f\nabla^2\Phi + f\right)$ is the absolute vorticity, ζ.

The first term on the right side of the equation is the differential vorticity advection term. It represents the rate of change with height of the advection of absolute vorticity. Increasing cyclonic vorticity advection with height leads to negative values of omega (upward motions) while increasing anticyclonic vorticity advection with height leads to positive values (downward motions). The second term represents the effect of the thermal (thickness) advection. In the absence of differential vorticity advection, omega will be negative when there is warm advection and positive for cold advection.

Trenberth (1978) has shown that equation (1) can be simplified to

$$(\nabla^2 + f_o^2/\sigma\, \partial^2/\partial p^2)\omega \approx 2f_o/\sigma\left[\, \partial V_g/\partial p \cdot \nabla\zeta\right] \qquad (2)$$

which qualitatively states that vertical motions can be determined visually from a chart containing thickness and vorticity contours by isolating areas where there is cyclonic vorticity advection by the thermal wind. Equation (2) can be utilized to quantitatively estimate omega values at 500 mb, for example, if 700-300 mb thickness and 500 mb vorticity patterns are known and if the left hand side of the equation can be integrated. The authors have utilized an approximation for the left hand side of (2) given by Holton (1979, p. 129). The solution of equation (2) was then programmed, in BASIC, on an Apple IIe microcomputer and utilized to obtain values of 500 mb omega for the present case.

Figure 19 shows the 700-300 mb thickness field and the NMC 500 mb vorticity pattern for 1200 UTC (0400 LST) on 24 September. A vorticity maximum is located just off the coast of Oregon with a strong vorticity gradient over Oregon and northern and central California. Over northern California, the vorticity gradient is almost perpendicular to a relatively strong thickness gradient. Therefore, one would expect that the greatest upward vertical velocities would be in northern California.

The omega analysis for 1200 UTC (0400 LST) is shown in Figure 20. It shows that a field of upward motions extended from southwestern Oregon to central California and, as expected, that the area of greatest upward motions was located over northern California. More significantly, it shows that the area of greatest upward motions was roughly colocated with the area where the Redding storm first developed.

Figure 21 shows the 700-300 mb thickness field and 500 mb vorticity field for 0000 UTC 25 September (1600 LST 24 September). Over east-central California and western Nevada, an area of relatively strong vorticity gradient is again nearly perpendicular to the thickness gradient so that the strongest upward vertical velocities would be expected in this area.

The omega analysis for this time (Figure 22) shows that the greatest upward motions are indeed over east-central California and western Nevada. At about this time, a line of strong thunderstorms was present southeast of Sacramento (Figures 12b and 13b), roughly under the upward motion center. Inferring the motion of the upward motion center from Figures 20 and 22 shows that the area of strongest upward motions moved southeast with the thunderstorms in the Central Valley or, in other words, that the most intense thunderstorms tended to exist under the area of maximum quasi-geostrophically induced upward motions.

B. Vertical Motions Stimulated By Jet Streak

i. Overview

The dynamic effects of upper tropospheric wind maxima, or jet streaks, in the production of severe weather occurrences in the Great Plains are well documented (McNulty, 1978; Uccellini and Johnson, 1979; Kloth and Davies-Jones, 1980; Bluestein and Thomas, 1984; Barnes and Newton, 1986; Schaefer et al., 1986; and, Bluestein, 1986). Riehl et al. (1954) and Reiter

(1967) have shown that upper tropospheric divergence related to ageostrophic accelerations is found in the left-front and the right-rear portions of a zonally-oriented dynamically-straight jet streak.

Qualitative interpretation of the divergence associated with such features becomes more difficult if the streak is not oriented zonally and if substantial curvature occurs in the flow. Since the Coriolis parameter is found in the denominator of the geostrophic wind relation, velocity convergence (divergence) will characterize that portion of the wind field which is geostrophic in northward (southward) flowing currents. This effect is small at the synoptic and mesoscales (Bluestein and Thomas, 1984) and does not interfere with the straightforward quadrature of divergence/convergence associated with jet streaks mentioned above.

The effects of curvature in the flow in generating strong centripetal accelerations can contribute substantially to alterations of the usual patterns of divergence and convergence in jet streaks. Bluestein and Thomas (1984) found that such curvature effects can be much more significant than all other factors in generating jet streak-related divergence patterns and cannot be neglected.

All complications aside, the horizontal divergence in the upper troposphere associated with jet streaks can create substantial vertical motions in the layers beneath. Bluestein and Thomas (1984) and Bluestein (1986) show that such vertical motions can be at least of the same order of magnitude as the vertical motions associated with the steady-state flow (for e.g., the usual upward velocities found on the eastern sides of migratory troughs in the westerlies).

ii. Jet Streak Analysis

It is beyond the scope of this study to intensively document the role that jet streak dynamics had in contributing to the development of the storms which eventually produced the tornadoes in the Sacramento Valley for this case. However, some simple calculations showed that such dynamic interactions were significant in this case.

Figure 23 is the NMC 300 mb height (decameters) and isotach (knots) patterns for 1200 UTC (0400 LST) 24 September 1986. The main trough axis extended from the Washington coastline southeastward through the Sacramento Valley and winds aloft in the storm genesis region were westerly. A jet streak, oriented from northwest to southeast, can be seen west of the Oregon coastline. Note that winds at the center exceeded 150 knots which classes this as an unusually strong feature for the season. The axis of the streak was located at the inflection point on the west side of the negatively-tilted short wave trough mentioned above.

The left front exit portion of the streak, which showed substantial curvature, was partially located over the storm genesis region of Northern California near the axis of the trough discussed in the last section. In such a situation, the area under the eastern portions of the trough frequently experiences stronger upwards vertical velocities than could be accounted for by the quasi-geostrophic effects discussed above. The usual explanation (see, for e.g., Kloth and Davies-Jones, 1980) is that as the jet streak moves around the axis of the trough, the divergence associated with the left front portion of the jet streak enhances the divergence found on the eastern portion of the trough. Because quasi-geostrophic theory only partially accounts for ageostrophic circulations associated with jet streaks, vertical velocities stronger than that expected from cyclonic vorticity advection by the thermal wind are characteristic.

The equations of motion for frictionless flow may be written

$$du/dt = f(v - v_g) \tag{3}$$

and

$$dv/dt = -f(u - u_g) \tag{4}$$

where u and v are the actual horizontal wind components and u_g and v_g are the geostrophic wind components.

Equations (3) and (4) can be used to estimate the accelerations which would be induced due to the ageostrophic flow associated with the jet streak where curvature effects are small and if the real wind observations are available. For this qualitative study, we assumed that the isotach and height analyses on Figure 23 were true representations of the conditions at 300 mb. We applied the equations at 40^{o}N, 125^{o}W where the curvature is small and slightly west of where the omega analyses summarized in the last section showed strong quasi-geostrophically induced upwards velocities. The net ageostrophic acceleration was towards the southwest with a magnitude of 8.88×10^{-4} m sec^{-2}. Such an acceleration imposed on an atmosphere initially in geostrophic balance with respect to the height contours (flowing from northwest to southeast) would result in a northeasterly component (cross-contour) to the flow of 38.4 m s^{-1} after 12 hr. While the actual magnitude of these accelerations and velocities must be viewed with caution, the nature of these results is what one would expect in this portion of the jet streak and suggests that ageostrophically-induced divergence would occur there in the absence of other effects.

We next tried to assess the qualitative nature of the divergence associated with the jet streak as a measure of the dynamic forcing which would have augmented the strong quasigeostrophic vertical velocities (see Figures 20 and 22) present over the storm genesis region. The vorticity equation may be written in the following manner if the tilting and solenoid terms are ignored:

$$d\zeta/dt = \partial\zeta/\partial t + V \cdot \nabla \zeta = - \zeta \, DIV_h \tag{5}$$

where ζ is the absolute vorticity and DIV_h is the horizontal divergence. Palmen and Newton (1969, p. 234) show that in the upper troposphere the vorticity tendencies are small compared to other terms and that the total change in vorticity can be approximated by the net advection term, or

$$d\zeta/dt = (V - C)\,\partial\zeta/\partial s \qquad (6)$$

where V is the magnitude of the wind, C is the translational speed of the pattern and $\partial\zeta/\partial s$ is the along stream vorticity gradient. Substitution of (6) into (5) will give an expression which will yield an estimate of the horizontal divergence.

$$DIV_h = -(V - C)/\zeta\,\partial\zeta/\partial s \qquad (7)$$

The vertical velocity, ω, at the level of non-divergence (LND) due to the jet streak may then be inferred from the simplified equation of continuity

$$\omega \approx DIV_{net} \int_{500}^{300} dp \qquad (8)$$

The procedure is of course fraught with dubious assumptions. To compute the vorticities required in equation (7) we assumed: (i) that the flow was basically straight so that all the relative vorticity was due to shear; and, (ii) that the NMC 300 mb isotach analysis (Figure 23) was an accurate portrayal of the real wind field. To use equation (8) to obtain an estimate of the jet streak induced vertical motions at 500 mb we made the assumptions that the calculated 300 mb divergence represented the mean divergence at the top of the layer bounded by 300 mb and the 500 mb level and that the LND was located at the 500 mb level.

Evaluation of equation (7) at 40°N, 125°W yielded a horizontal divergence of 2.5 X 10^{-5} sec^{-1}. Insertion of this value into equation (8) yielded a ageostrophically-induced ω of -5.1 μb s^{-1}. While we again caution that these numerical estimates should only be thought of as gross approximations, we point out that at a qualitative level the jet streak-induced vertical motions were of the same order of magnitude of those induced quasi-geostrophically (see Figures 20 and 22).

By 0000 UTC 25 September 1986 (1600 LST 24 September 1986) (Figure 24), the jet streak had weakened (although the strongest winds still exceeded 130 knots) and had progressed southeastward. Since the left front quadrant of the streak was then positioned over the San Joaquin Valley where quasi-geostrophically induced upwards vertical velocities where located, one could assume that ageostrophic augmentation of vertical velocities had shifted to that region by afternoon.

VIII. DISCUSSION

The genesis and life cycle of the thunderstorm which produced an outbreak of tornadoes near Vina, CA on 24 September 1986 compares favorably in many respects to that which is expected

to occur for the typical supercell thunderstorm in the Great Plains. This is remarkable to the extent that such storms have been thought to be rare or absent features in the climatology of California, a view which has given considerable inertia to the idea that such storms simply CANNOT occur here.

Some of the evidence presented here is somewhat circumstantial and, to a certain extent, quantitatively dubious. However, since whatever inaccuracies inherent in the analyses have to do with magnitudes and not the basic nature of calculated quantities, the qualitative evidence presented here is compelling.

The storm formed in convectively unstable air and in a favorably sheared environment. The genesis was dynamically aided by quasigeostrophically-induced vertical motions associated with a progressing trough in the westerlies and ageostrophically-induced vertical motions associated with a jet streak. These motions occurred simultaneously over the northern Sacramento Valley in the early morning hours of the 24th. The surface flow in that region was subjected to horizontal convergence and vertical stretching as it flowed northward through the Valley ahead of a post-frontal surface trough. Thus, the vertical motion field was acting on an air mass which was destabilizing for four reasons: i. lifting due to horizontal convergence; ii. lifting due to increasing elevation in transit of the convectively unstable air northward through the Valley; iii. diurnal heating; and, iv. advection of moisture from the south in the lowest layers. In addition, destabilization was occurring all over the region because of differential temperature advection.

A large gradient in surface dew point temperatures existed across the developing storm. Streamline analyses show that the drier air originated both from the rear flank downdraft associated with the storm complex and from Pacific air subsiding to the lee of the coastal mountain ranges. The moist air was being brought northward by strong surface southeasterly winds. The Redding storm moved to the right of the mean tropospheric wind in such a fashion that its southwestern flank was continually being supplied by the moist air flow from the southeast.

The F2 tornado near Vina (and the weaker tornado near Stockton) developed shortly after collapse of the overshooting top. At that time, the storm had a classical wall cloud with evidence that a clear slot had developed to the west of the funnels. The downdraft suggested by the clear slot may have been responsible for the lowlevel drying upwind of the storm. In any case, as it moved south-southeastward the storm remained on the moist air side of the boundary between the drier Pacific air and the moister southeasterly flow. This behavior was similar to that of dry-line type severe thunderstorms observed in the Great Plains.

IX. CONCLUSIONS

In an extensive and lucid treatment of the mesometeorology of severe weather, Doswell (1982) pointed out that the key to anticipating the development of severe storms is to understand how the given pattern contributes to adequate air mass destabilization, and favorable low level moisture and upwards vertical motion fields. He emphasizes that once the operational meteorologist is able to diagnose the situation on these bases, it is not necessary to consult a list of rules to decide on the forecast. Although his remarks were directed to those involved in severe weather forecasts in the central portion of the United States, he states that no matter what the season or what the location, when such patterns duplicate, then severe weather can be anticipated.

The tornadic storm examined in this study is a case in point. With the advantage of hindsight, it seems clear that severe thunderstorms were likely to occur somewhere in the Sacramento Valley on 24 September. The evidence is clear that many of the factors present in the development of supercell thunderstorms in the Great Plains were acting in concert over the Valley in this case.

With reference to the present study, the authors concede that much more detailed quantitative work is needed, particularly in investigation of the role of the jet streak in instigating vertical motions. Enough compelling evidence was presented, however, to suggest that forecasters in California should have a working knowledge of severe weather dynamics.

Finally, the authors feel that synoptic pattern recognition is a technique which has fallen into disuse in recent years. We have endeavored to point out that the pattern which contributed to the severe weather in this case is one which has been identified previously in the literature as favorable for severe weather on the West Coast. The violent weather associated with this case underscores the need for operational meteorologists to be thoroughly schooled in such patterns and their implications.

X. ACKNOWLEDGEMENTS

The authors gratefully acknowledge the help of many individuals associated with the National Weather Service in making this study possible. We particularly would like to thank Mr. Glenn Rasch (Chief, Scientific Services Division (SSD), Western Region, Salt Lake City, UT) and Dr. Joseph T. Schaefer (Chief, SSD, Central Region, Kansas City, MO) for suggesting publication of this study and for reviewing the manuscript. In addition, Dr. Charles Doswell III (Research Meteorologist, National Severe Storms Lab, Norman, OK), Mr. Jack Hales (Lead Forecaster, NSSFC, Kansas City, MO) and Mr. Ken Mielke (Assistant Chief, SSD, Western Region, Salt Lake City, UT) also acted as reviewers and provided the authors with many valuable suggestions on how to improve the manuscript. Mr. Dan Guido (Forecaster, National Weather Service Forecast Office (WSFO), Salt Lake City, UT) supplied the authors with hodographs and satellite images. Mr. Chris Fontana (Meteorologist-in-charge, WSO, Redding, CA) provided the photographs of the Vina tornado and Mr. Donald Maker (Official-in-charge, WSO, Stockton, CA) supplied supplementary weather observations. We thank Mr. E. Jan Null (Lead Forecaster, WSFO, Redwood City, CA) and Mr. Jim Henderson (Deputy Director, Central Region, Kansas City, MO) for encouraging us in this project. Finally, the study of severe thunderstorms would not be possible without the field support given to academics by personnel of the NWS. The authors would like to acknowledge the support given storm chasers from San Francisco State University by Mr. Robert Landis (Director, Southern Region, Fort Worth, TX) and by the staff of many WSFOs and WSOs throughout the Southern and Central Regions.

This research was partially supported by internal grants from the School of Science and the Department of Geosciences, San Francisco State University.

XI. REFERENCES

Barnes, S., 1987: Analysis of quasi-geostrophic forcing during the AIMCS project - Volume I: Discussion. NOAA Tech. Memo. ERL ESG-27, 31 pp. [Available from National Severe Storms Lab, Norman, OK.]

_____, 1986: On the accuracy of omega diagnostic computations. MON. WEA. REV., **114**, 1664-1680.

_____, and C.W. Newton, 1986: Thunderstorms in the synoptic setting. In Thunderstorm morphology and dynamics, Second Edition, edited by E. Kessler, University of Oklahoma Press, Norman, OK., 75-112.

_____, 1985: Omega dianostics as a supplement to LFM/MOS quidance in weakly forced convective situations. MON. WEA. REV., **113**, 2122-2141.

Bluestein, H.B., 1986: Fronts and jet streaks: a theoretical perspective. In Mesoscale meteorology and forecasting, edited by Peter Ray, AMS, Boston, 173-215.

_____, and K. Thomas, 1984: Diagnosis of a jet streak in the vicinity of a severe weather outbreak in the Texas Panhandle. MON. WEA. REV., **112**, 2499-2519.

_____, 1979: A mini-tornado in California. MON. WEA. REV., **107**, 1227-1229.

Browning, K. A., 1986: Morphology and classification of middle-latitude thunderstorms. In Thunderstorm morphology and dynamics, Second Edition, edited by E. Kessler, University of Oklahoma Press, Norman, OK., 133-153.

Carlson, T.N., S.G. Benjamin, G.S. Forbes, and Y.F. Li, 1983: Elevated mixed layers in the regional severe storm environment: Conceptual model and case studies. MON. WEA. REV., **111**, 1453-1473.

Chisholm, A.J., and J.H. Renick, 1972: The kinematics of multicell and supercell Alberta hailstorms. Alberta Hail Studies, 1972, Research Council of Alberta Hail Studies Rep. No. 72-2, pp. 24-31.

Cooley, J., 1978: Cold air funnel clouds. MON. WEA. REV., **106**, 1368-1372.

Court, A., 1974: The climate of the coterminous United States. In Climates of North America, World Survey of Climatology, Vol. 11, Elsevier, New York, 193-343.

Davies-Jones, R., 1986: Tornado dynamics. In Thunderstorm Morphology and Dynamics, Second Edition, Edited by W. Kessler. University of Oklahoma Press, Norman, 197-236.

Doswell, C.A. III, 1987: The distinction between large-scale and mesoscale contribution to severe convection: a case study example. WEA. FORE., **2**, 3-16.

_____, 1986: Short range forecasting. In Mesoscale meteorology and forecasting, edited by Peter Ray, AMS, Boston, 689-719.

_____, 1985: The operational meteorology of convective weather - Volume II: storm scale analysis. NOAA Tech. Memo. ERL ESG-15, 240 pp. [Available from National Severe Storms Lab, Norman, OK.]

_____, 1982: The operational meteorology of convective weather - Volume 1: operational mesoanalysis. NOAA Tech. Memo. NWS NSSFC-5, 172 pp. [Available from National Severe Storms Lab, Norman, OK.]

Durran, D.R., and L.W. Snellman, 1987: The diagnosis of synoptic-scale vertical motion in an operational environment. WEA. FORE., **2**, 17-31.

Fawbush, E. and R. Miller, 1954: The types of air masses in which North American tornadoes form. BULL. AMER. METEOR. SOC., **35**, 154-165.

Fontana, C., 1986: Report from the Redding, CA office of the National Weather Service on the Vina Tornado of 24 September 1986. Available from National Weather Service Forecasting Office, 660 Price Ave., Redwood City, CA 94063.

_____, 1977: Study of a heavy precipitation occurrence in Redding, California. NOAA Tech. Memo. NWS WR-123, 19 pp. [Available from National Weather Service Western Region Headquarters, Salt Lake City, UT.]

Hales, J., 1985: Synoptic features associated with Los Angeles tornado occurrences. BULL. AMER. METEOR. SOC., **66**, 657-662.

_____, and C. Doswell III, 1982: High resolution diagnosis of instability using hourly surface lifted parcel temperatures. Preprints, 12th AMS Conference on Severe Local Storms, San Antonio, TX, 172-175.

Halvorson, D.A., 1971: Tornado and funnel clouds in San Diego County. WESTERN REGION TECHNICAL ATTACHMENT No. 71-33. National Weather Service Western Region, PO Box 11188, Salt Lake City, Utah 84147.

Heflick, S., and J. Fors, 1979: A simple analysis/diagnosis system for real time evaluation of vertical motion. NOAA Tech. Memo. NWS WR-138, 27 pp. [Available from National Weather Service Western Region Headquarters, Salt Lake City, UT.]

Holmes, K.A., 1984: Cold air funnels never touch down? WESTERN REGION TECHNICAL ATTACHMENT No. 84-10. National Weather Service Western Region, PO Box 11188, Salt Lake City, Utah 84147.

Holton, J., 1979: An Introduction to Dynamic Meteorology, Second Edition. Academic Press, 391 pp.

Kloth, C.M., and R.P. Davies-Jones, 1980: The relationship of the 300-mb jetstream to tornado occurrence. NOAA Environmental Research Laboratories, Natl. Severe Storms Lab, Tech. Memo. ERL NSSL-88, 62 pp. [Available from National Severe Storms Lab, Norman, OK.]

Lacy, R.E., 1968: Tornadoes in Britain during 1963-1966. WEATHER, 23, 116-124.

Lemon, L. and C. Doswell III, 1979: Severe thunderstorm evolution and mesocyclone structure as related to tornadogenesis. MON. WEA. REV., **107**, 1184-1197.

Lussky, G.R., 1986: The MCC - an overview and case study on its impact in the Western United States. NOAA Tech. Memo. NWS WR-193, 50 pp. [Available from National Weather Service Western Region Headquarters, Salt Lake City, UT.]

Marwitz, J.D., 1972: The structure and motions of severe hailstorms: I, Supercell storms. J. APPL. METEOROL., **11**, 166-179.

McNulty, R., 1978: On upper troposhperic kinematics and severe weather occurrence. MON. WEA. REV., **106**, 662-672.

Monteverdi, J.P., S.A. Braun, and T.C. Trimble, 1988: Funnel clouds in the San Joaquin Valley, California. MON. WEA. REV., **116**, 782-789.

_____, 1976: The single air mass disturbance and precipitation characteristics at San Francisco. MON. WEA. REV., **104**, 1289-1296.

Mullen, S., 1979: An investigation of small synoptic scale cyclones in polar air streams. MON. WEA. REV., **107**, 1636-1647.

Ninomiya, K., 1971: Mesoscale modification of synoptic situations from thunderstorm development as revealed by ATS III and aerological data. J. APPL. METEOR., **10**, 1103-1121.

NOAA, 1984a: Cold air funnels - Hill AFB. WESTERN REGION TECHNICAL ATTACHMENT No. 84-20. [Available from National Weather Service Western Region Headquarters, Salt Lake City, UT].

_____, 1984b: Convective stability indices. WESTERN REGION TECHNICAL ATTACHMENT No. 84-14. [Available from National Weather Service Western Region Headquarters, Salt Lake City, UT].

Petterssen, S., 1956: Weather Analysis and Forecasting, Second Edition, Volume 1. McGraw-Hill Book Company, Inc., 428 pp.

Randerson, D., 1986: A mesoscale convective complex type storm over the desert Southwest. NOAA Tech. Memo. NWS WR-196, 54 pp. [Available from National Weather Service Western Region Headquarters, Salt Lake City, UT.]

Reed, R., and W. Blier, 1986: A case study of comma cloud development in the Eastern Pacific. MON. WEA. REV., **114**, 1681-1695.

_____, 1979: Cyclogenesis in polar air streams. MON. WEA. REV., **107**, 38-52.

Reiter, E.R., 1967: Jet streams. Doubleday & Co., Inc., New York, 178 pp.

Riehl, H., M.A. Alaka, C.L. Jordan, and R.J. Renard, 1954: The Jetstream. METEOR. MONOGR., **2**, No. 7, American Meteorological Society, Boston, 54 pp.

_____, 1954: Tropical Meteorology. McGraw-Hill Book Company, 392 pp.

Schaefer, J.T., L.R. Hoxit, and C.F. Chappell: Thunderstorms and their mesoscale environment. In Thunderstorm morphology and dynamics, Second Edition, edited by E. Kessler, University of Oklahoma Press, Norman, OK., 113-132.

Smith, T.B., 1971: Estimates of maximum wind speeds of tornadoes in California. Rep. to So. Cal. Edison, Los Angeles by Meteorology Research Inc., 464 W. Woodbury Rd., Arcata, 14 pp.

Trenberth, K., 1978: On the interpretation of the diagnostic quasi-geostrophic omega equation. MON. WEA. REV., **106**, 131-137.

Uccellini, L. and D. Johnson, 1979: The coupling of upper and lower tropospheric jet streaks and implications for the development of severe convective storms. MON. WEA. REV., **107**, 682-703.

U.S.D.C., 1986: Storm Data--California, Vol 28, No. 9. National Climatic Data Center, Asheville, N.C. 28801.

Weaver, R. L., 1962: Meteorology of hydrologically critical storms in California. U.S. Weather Bureau, Hydrologic Services Division, Hydrol. Rep. No. 37, Washington, D.C., 207 pp.

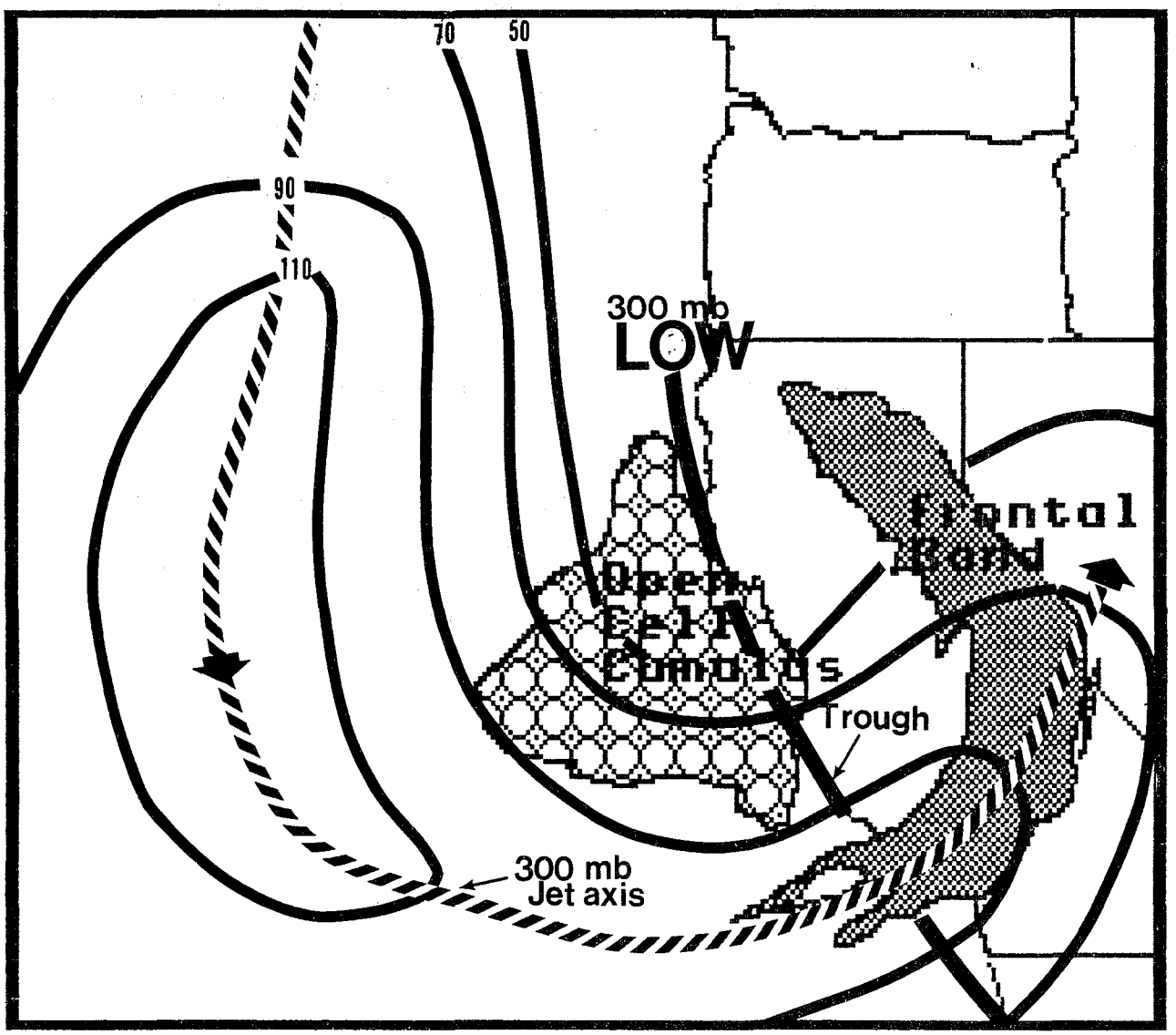

Figure 1 Schematic diagram showing the location of cloud features in relation to 300 mb trough and jet streak axes for 21 March 1987 when funnel clouds were observed in the San Joaquin Valley.

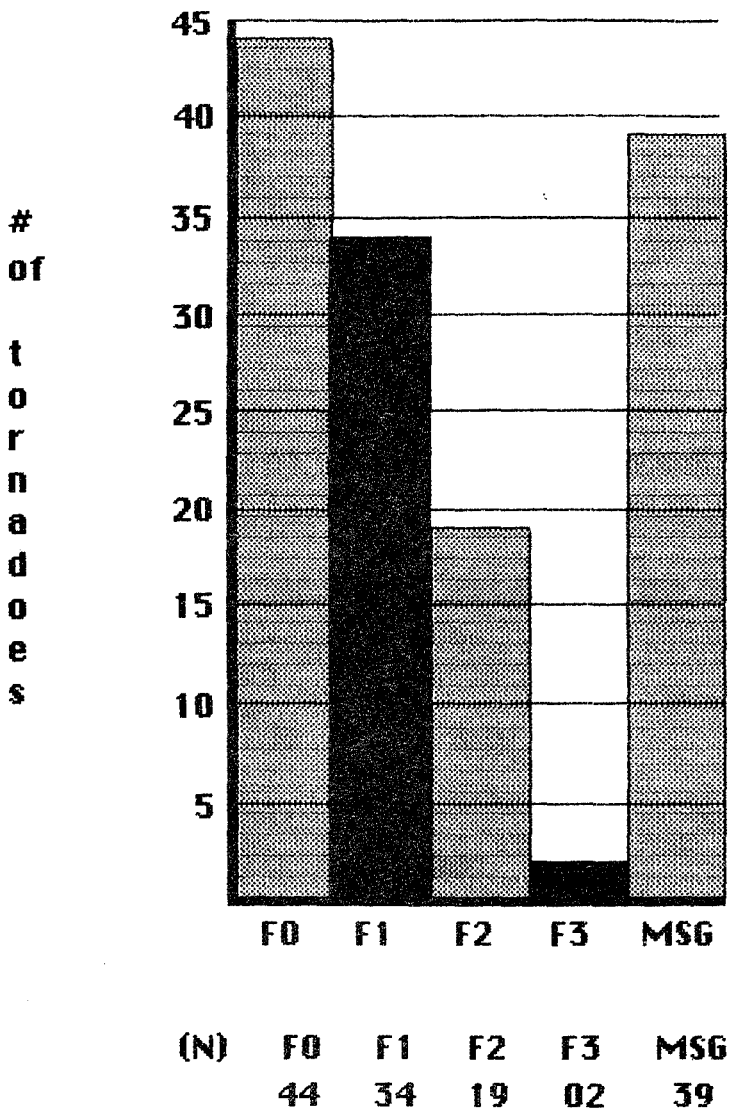

Figure 2. Tornado distribution by F-scale intensity for all tornadoes in California during the period 1950-1986.

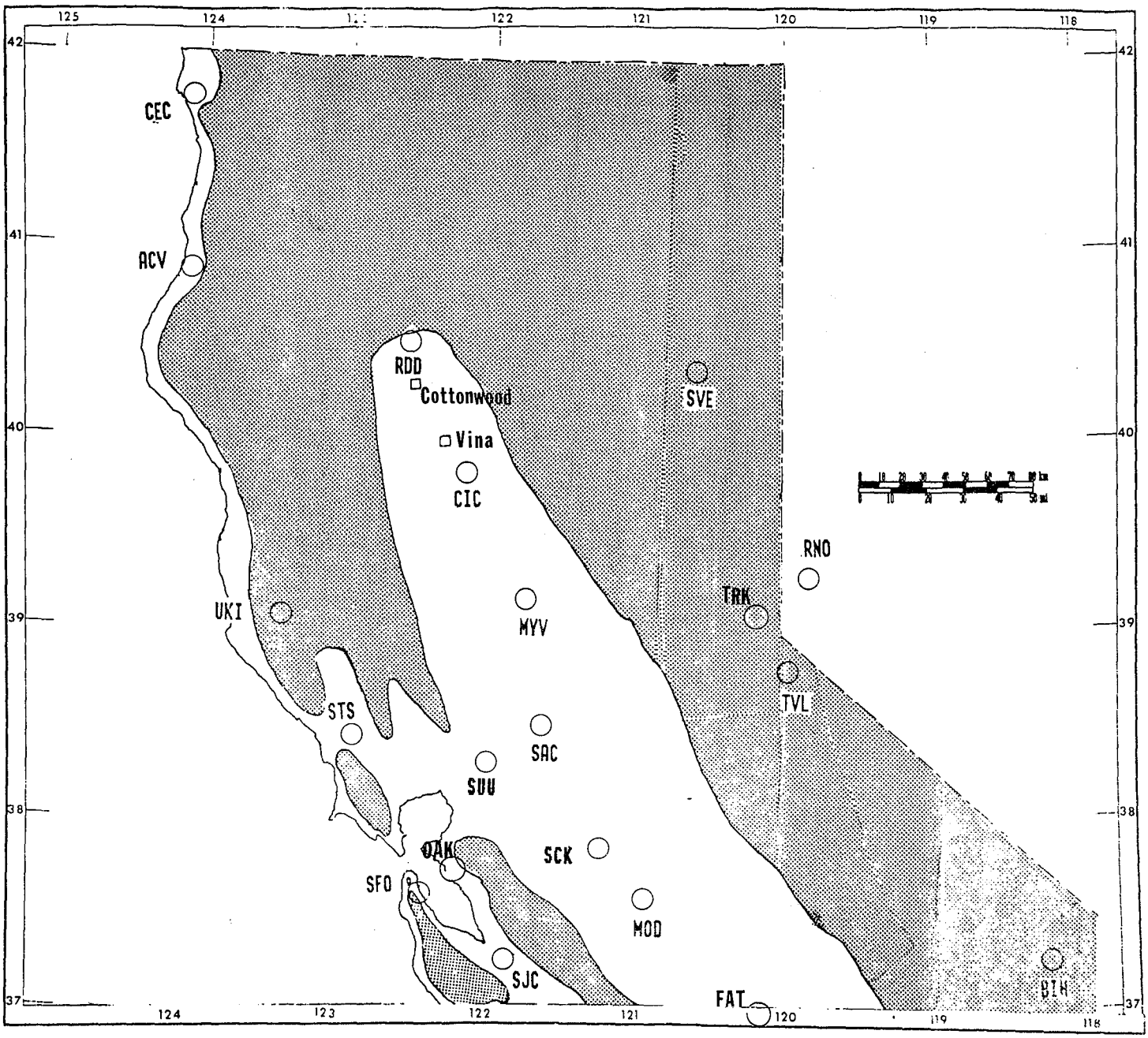

Figure 3. Station location map.

Figure 4a. Photograph of tornado near Vina, CA at approximately 2015 UTC (1215 LST) 24 September 1986.

Figure 4b. As in Figure 4a, except for 2020 UTC (1220 LST).

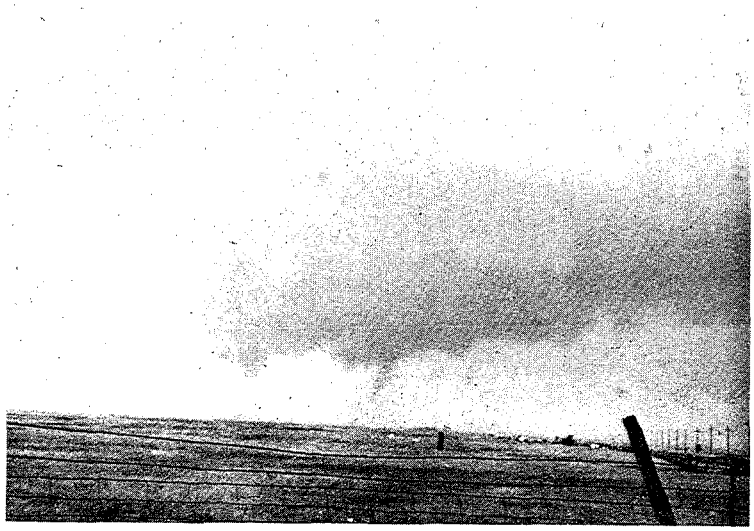

Figure 4c. As in Figure 4a, except for 2025 UTC (1225 LST).

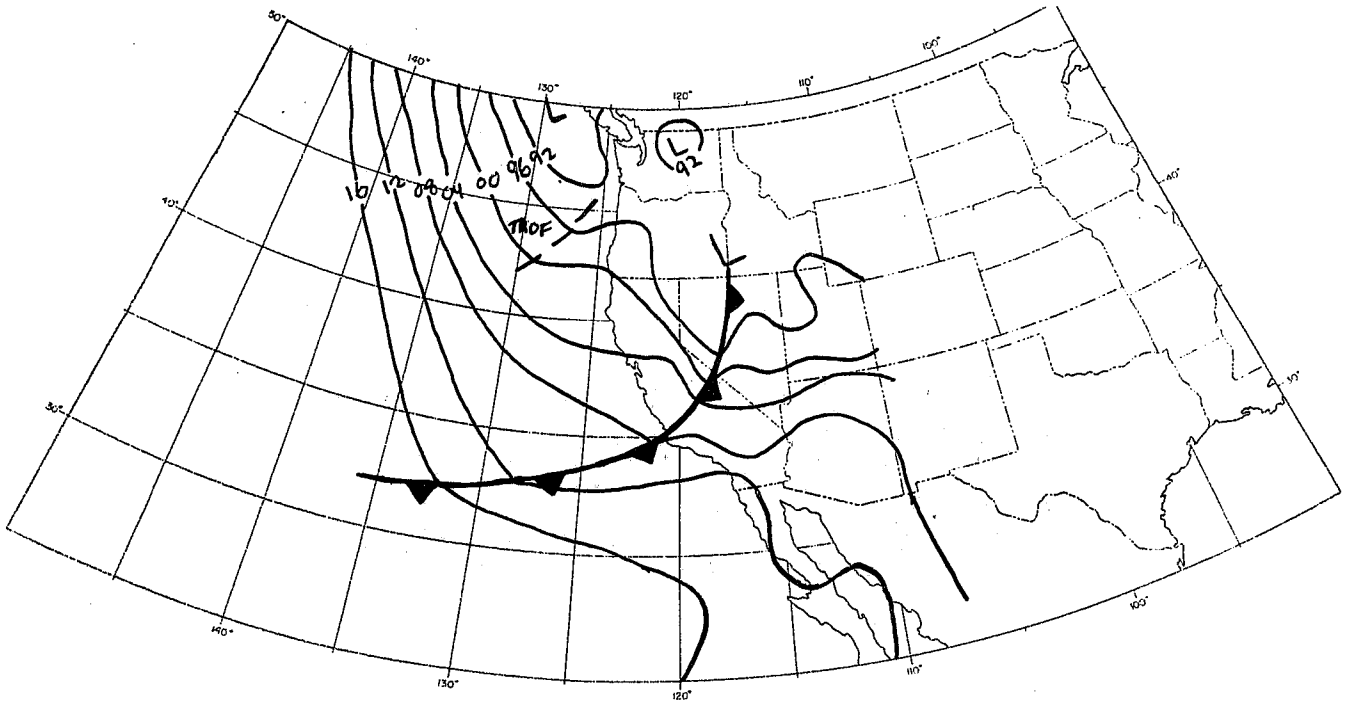

Figure 5. Surface map for 1800 UTC (1000 LST) 24 September 1986.

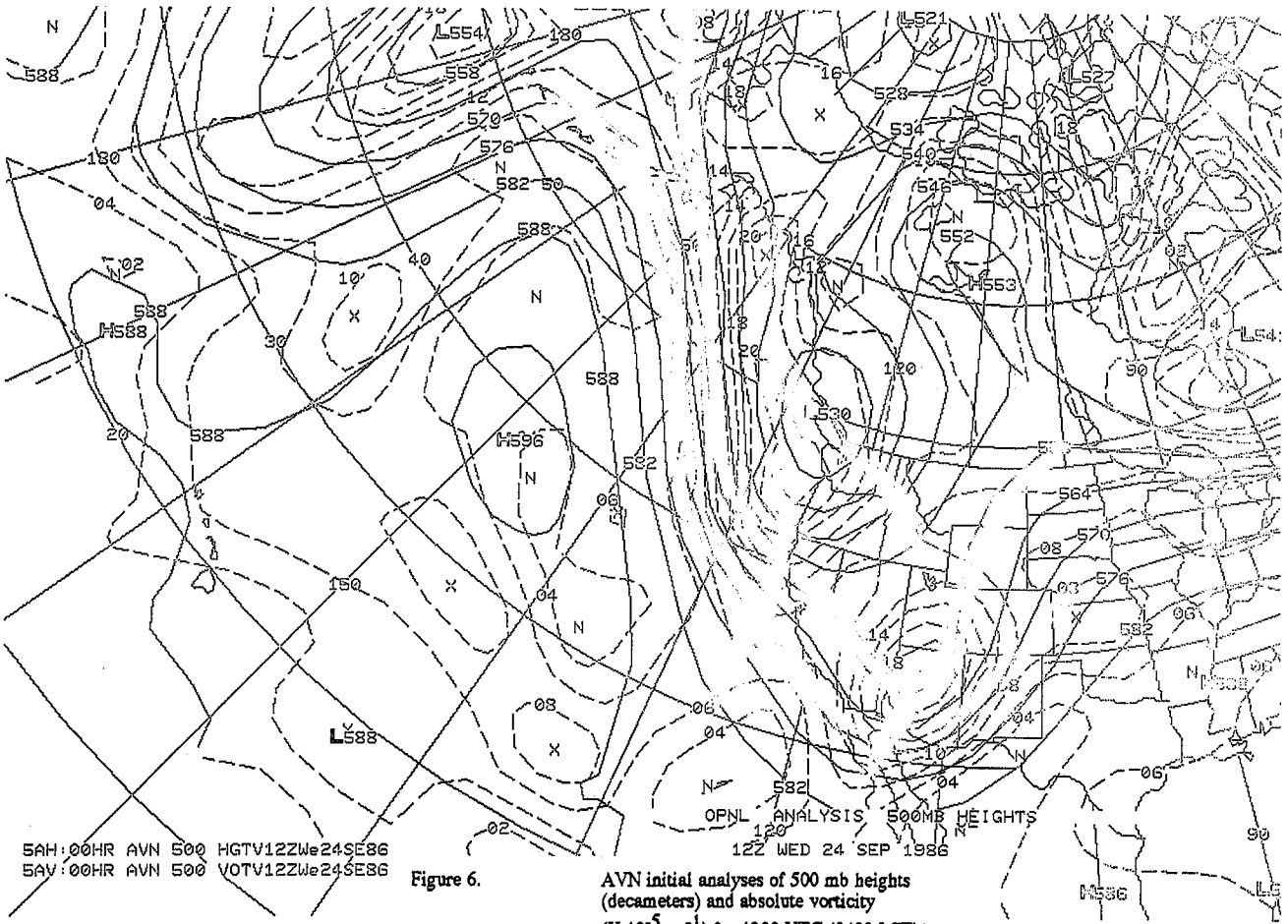

Figure 6. AVN initial analyses of 500 mb heights (decameters) and absolute vorticity ($X\ 10^{-5}sec^{-1}$) for 1200 UTC (0400 LST) 24 September 1986.

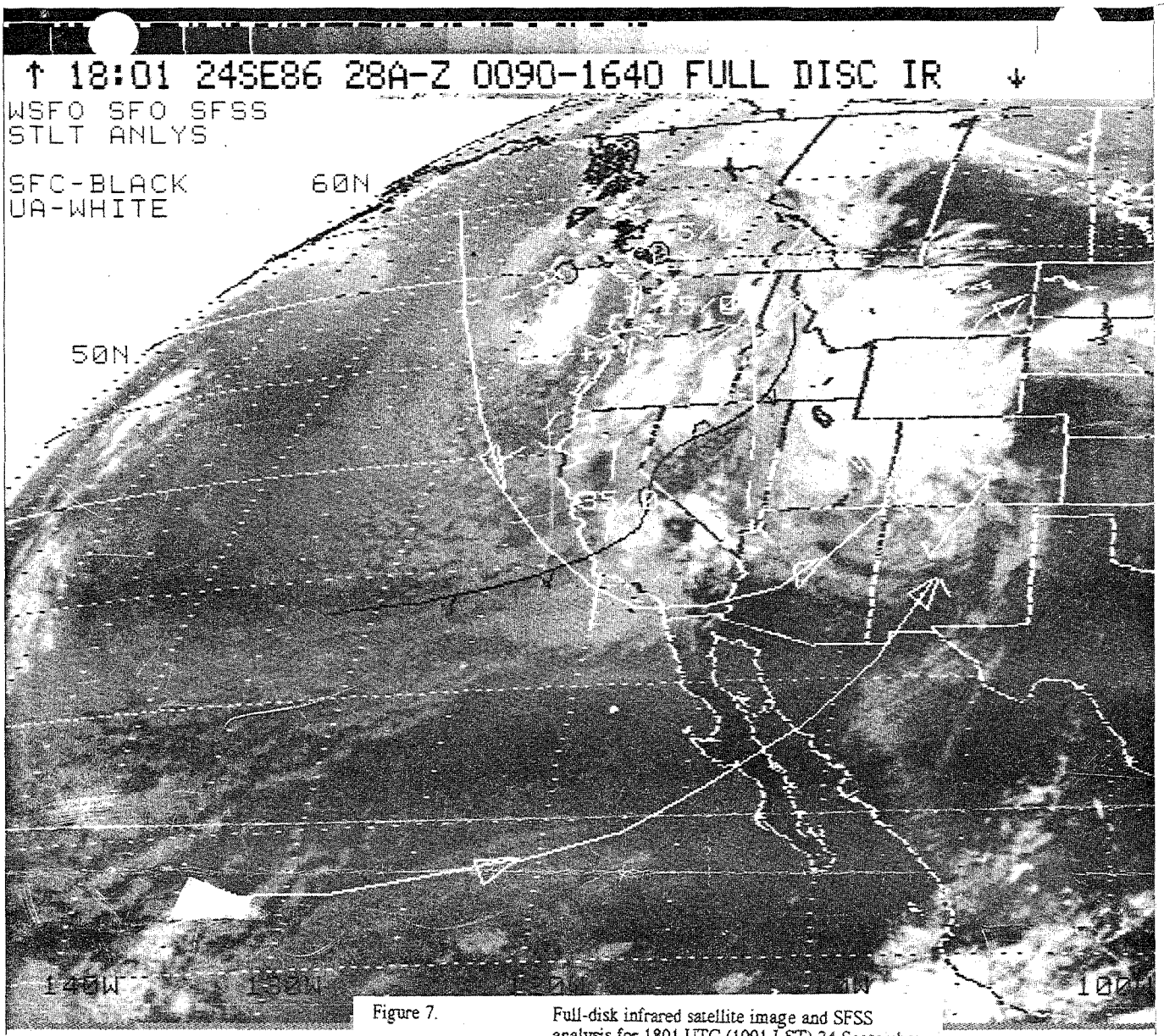

Figure 7. Full-disk infrared satellite image and SFSS analysis for 1801 UTC (1001 LST) 24 September 1986.

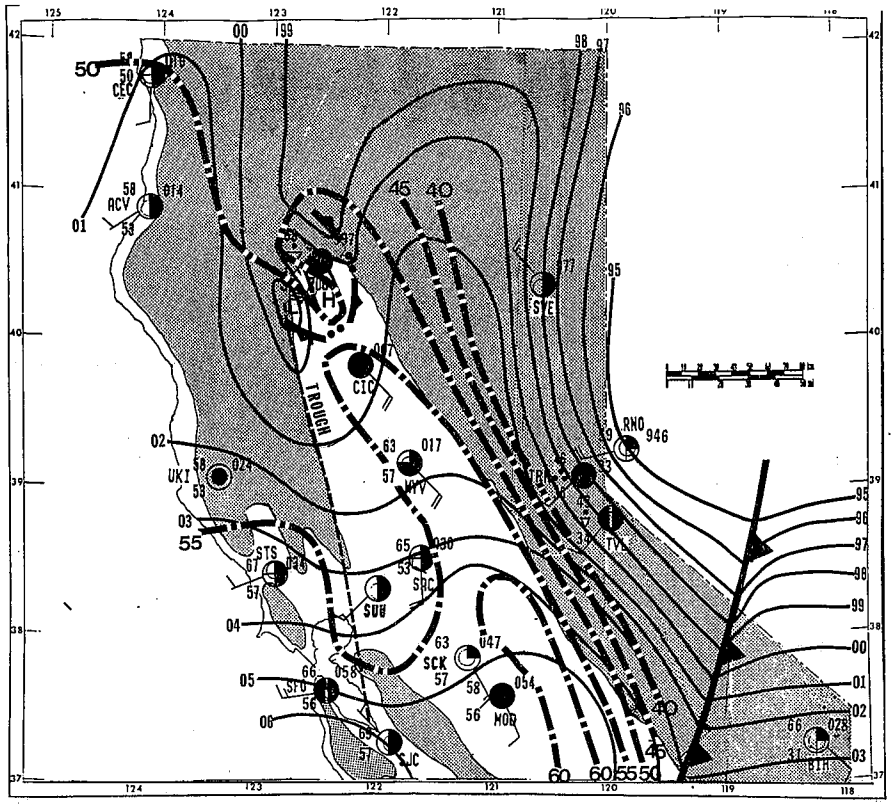

Figure 8a. Surface mesoanalysis for 1900 UTC (1100 LST) 24 September 1986.

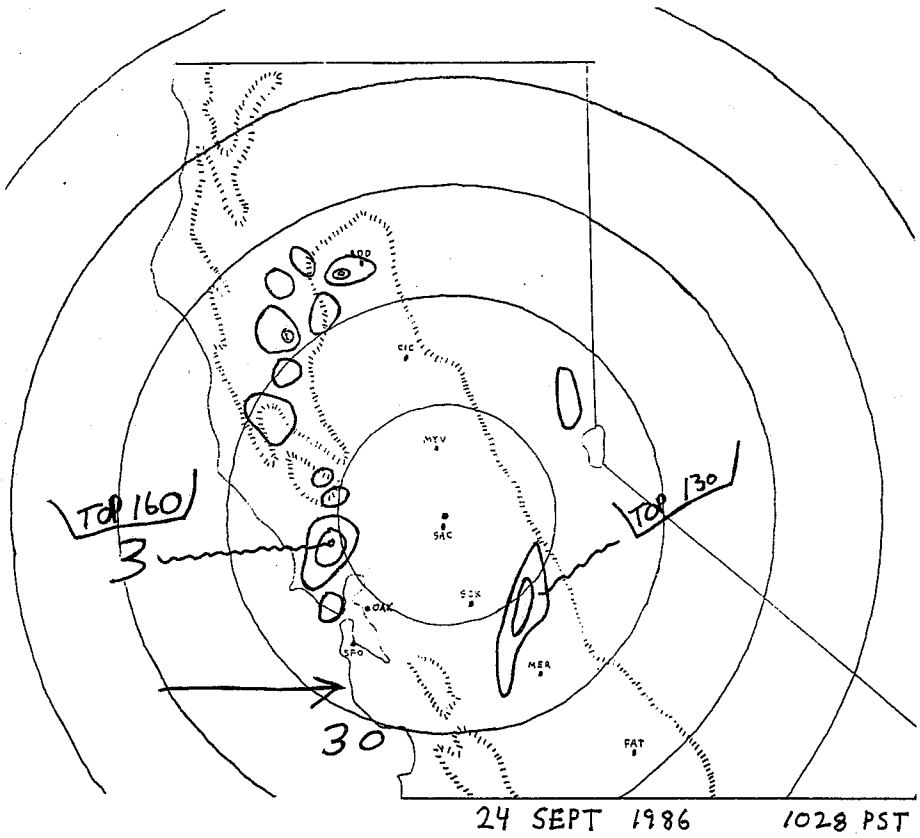

Figure 8b. Facsimile of Sacramento WSR-57 Plan Position Indicator Scope for 1828 UTC (1028 LST) 24 September 1986.

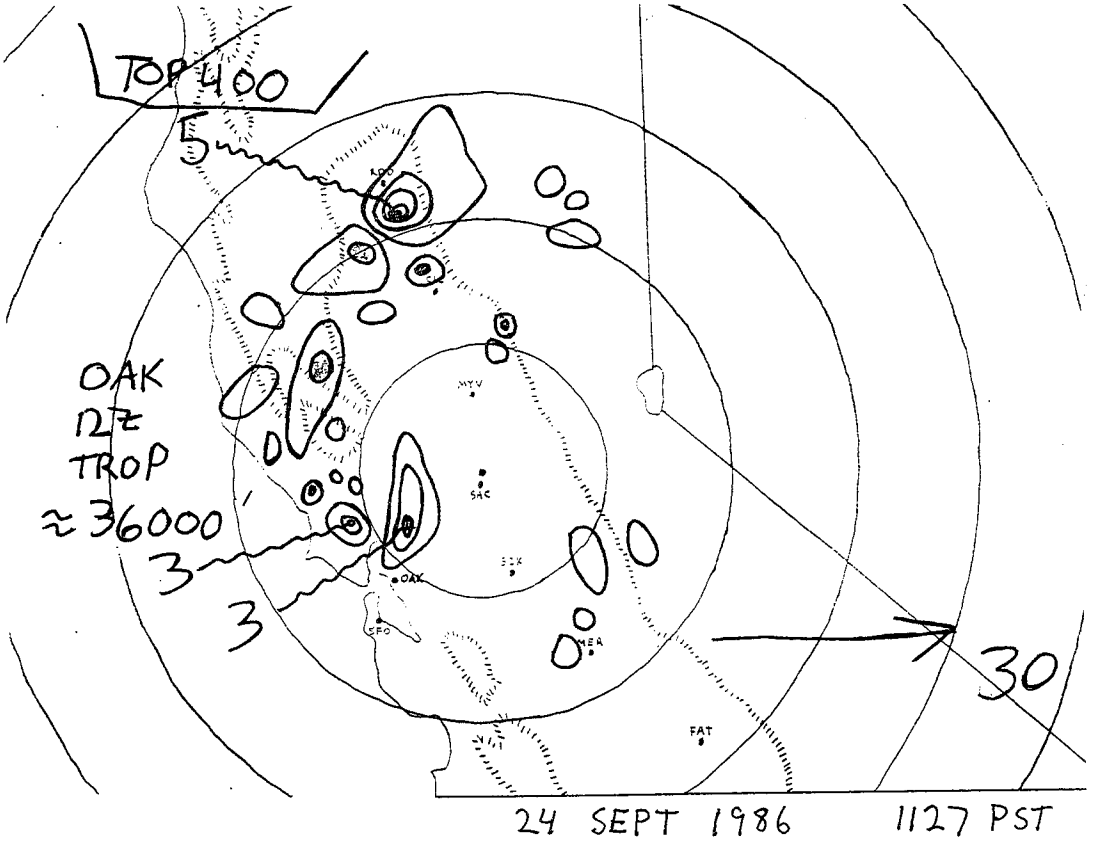

Figure 8c. As in Figure 8b, except for 1927 UTC (1127 LST).

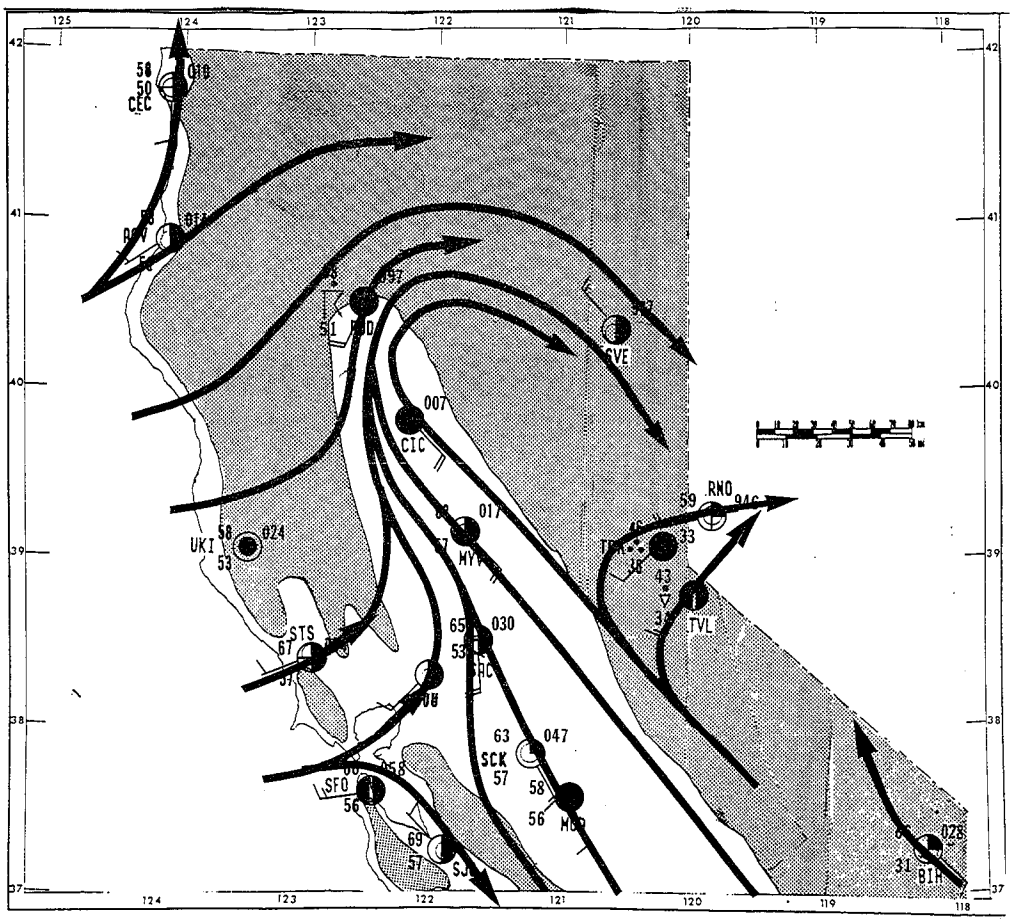

Figure 8d. Surface streamline analysis for 1900 UTC (1100 LST) 24 September 1986.

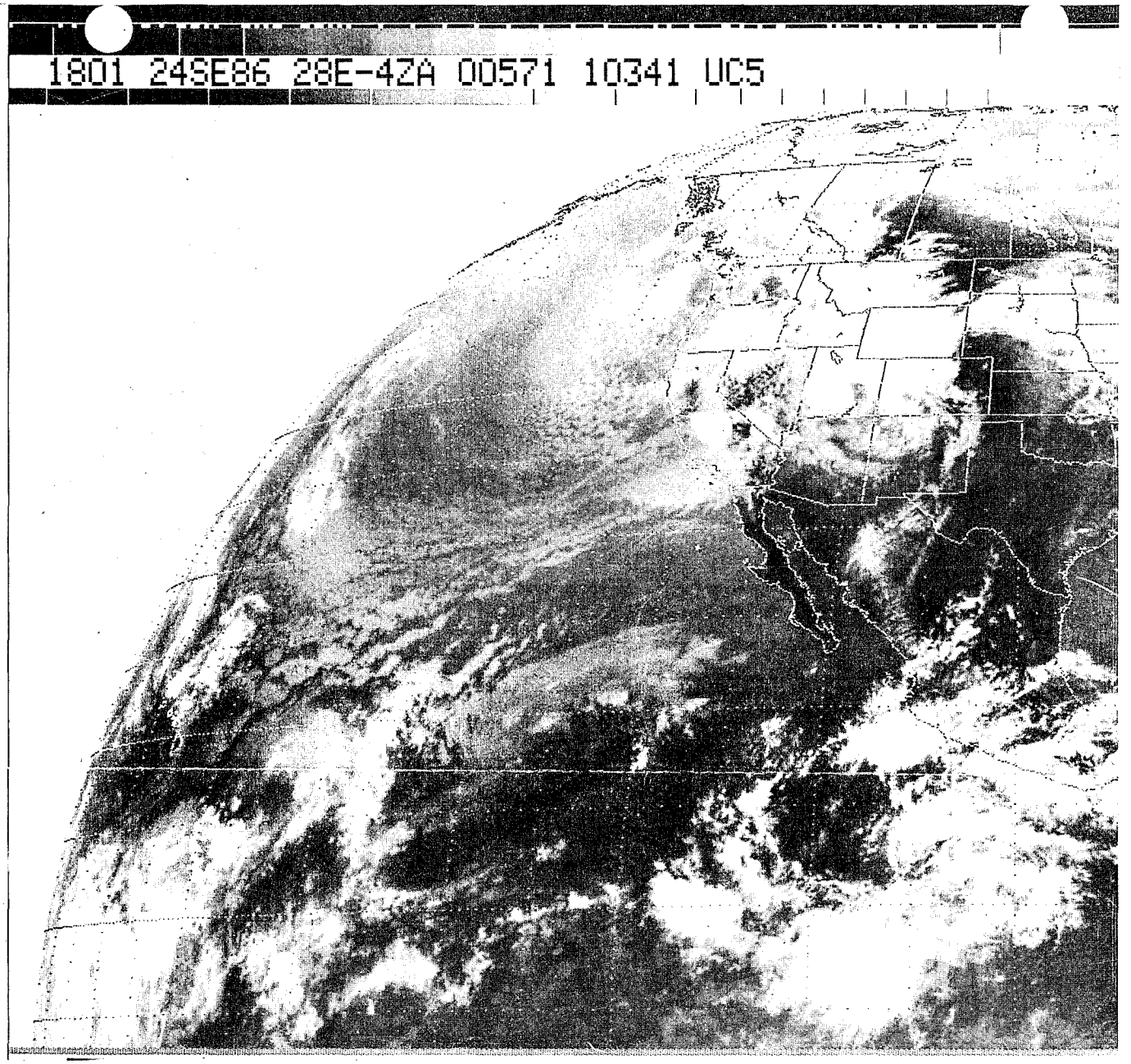

Figure 8e. Hemispheric infrared satellite image for 1801 UTC (1001 LST) 24 September 1986.

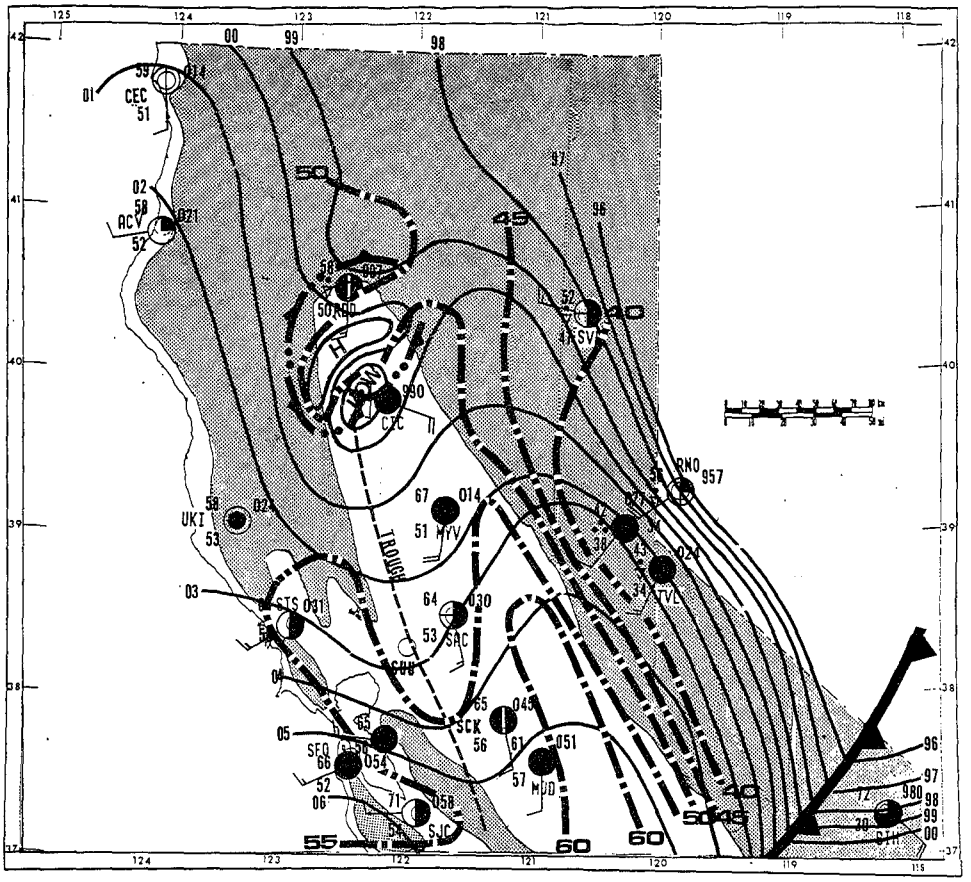

Figure 9a. As in Figure 8a, except for 2000 UTC (1200 LST).

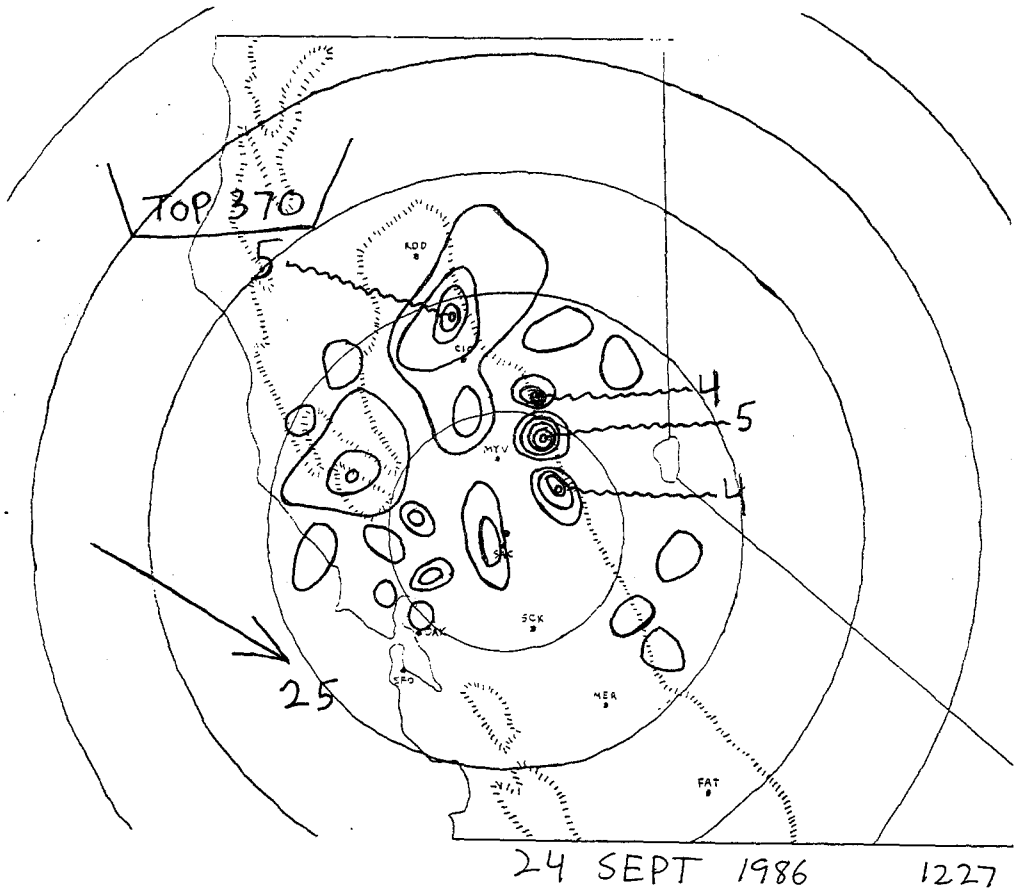

Figure 9b. As in Figure 8b, except for 2027 UTC (1227 LST).

Figure 9c. As in Figure 8d, except for 2000 UTC (1200 LST).

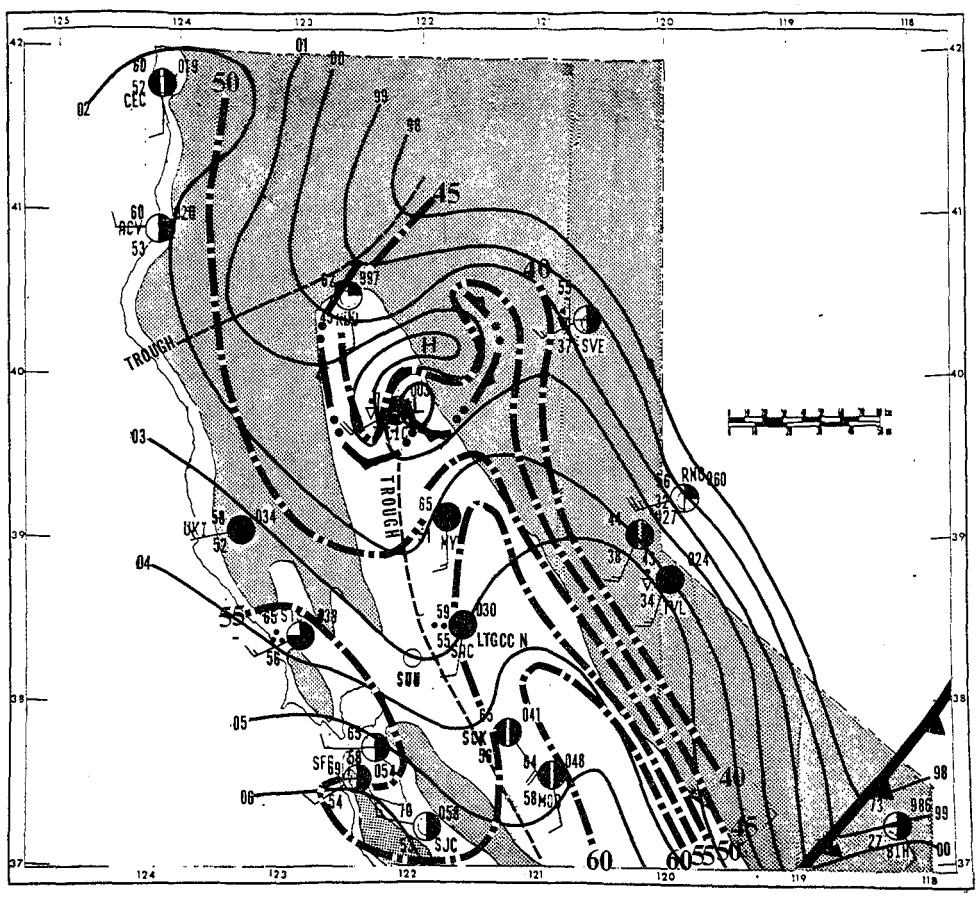

Figure 10a. As in Figure 8a, except for 2100 UTC (1300 LST).

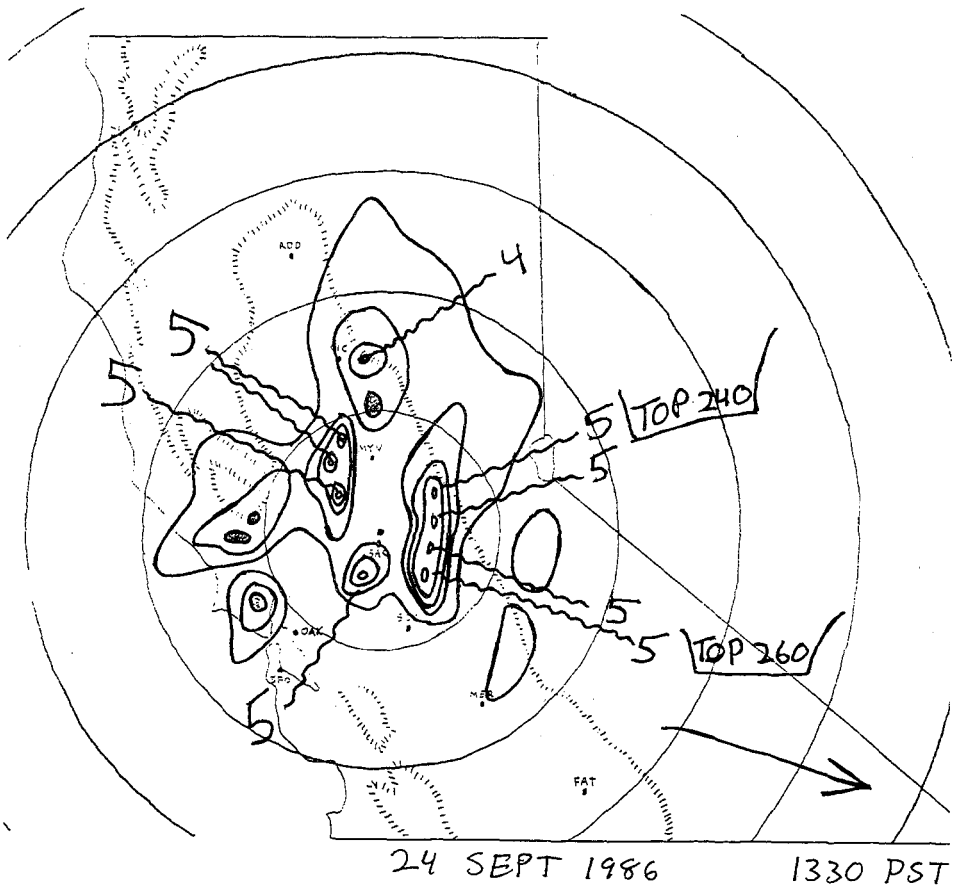

Figure 10b. As in Figure 8b, except for 2130 UTC (1330 LST).

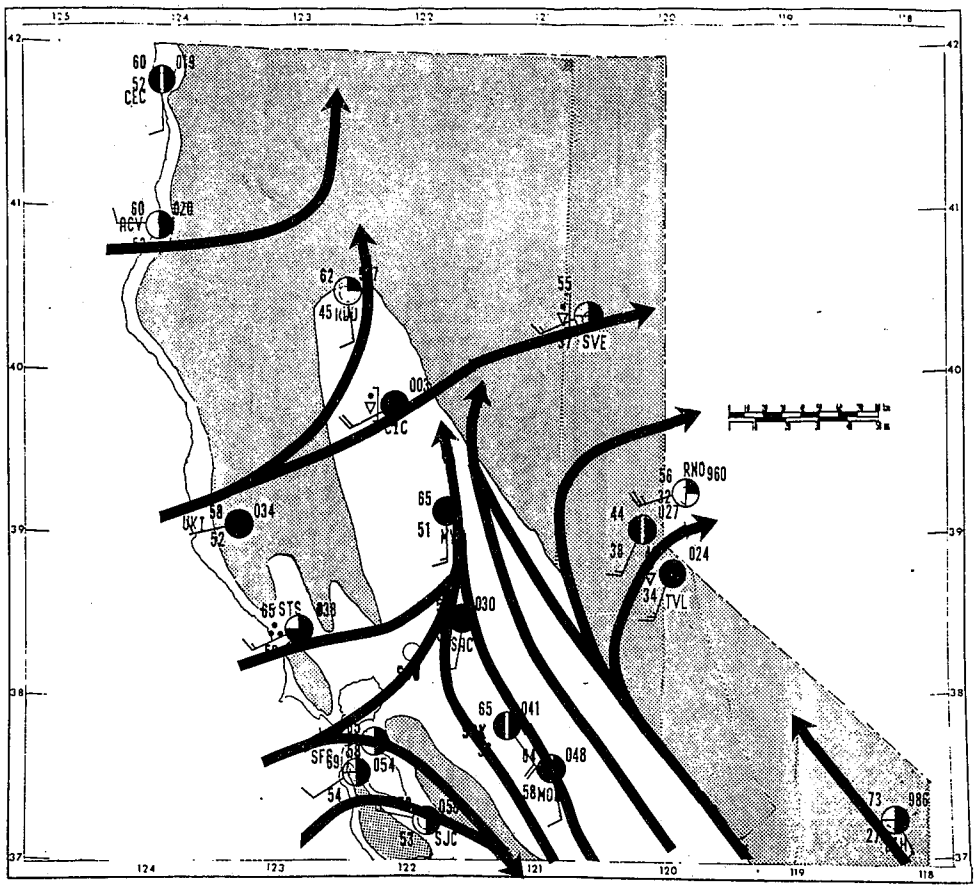

Figure 10c. As in Figure 8d, except for 2100 UTC (1300 LST).

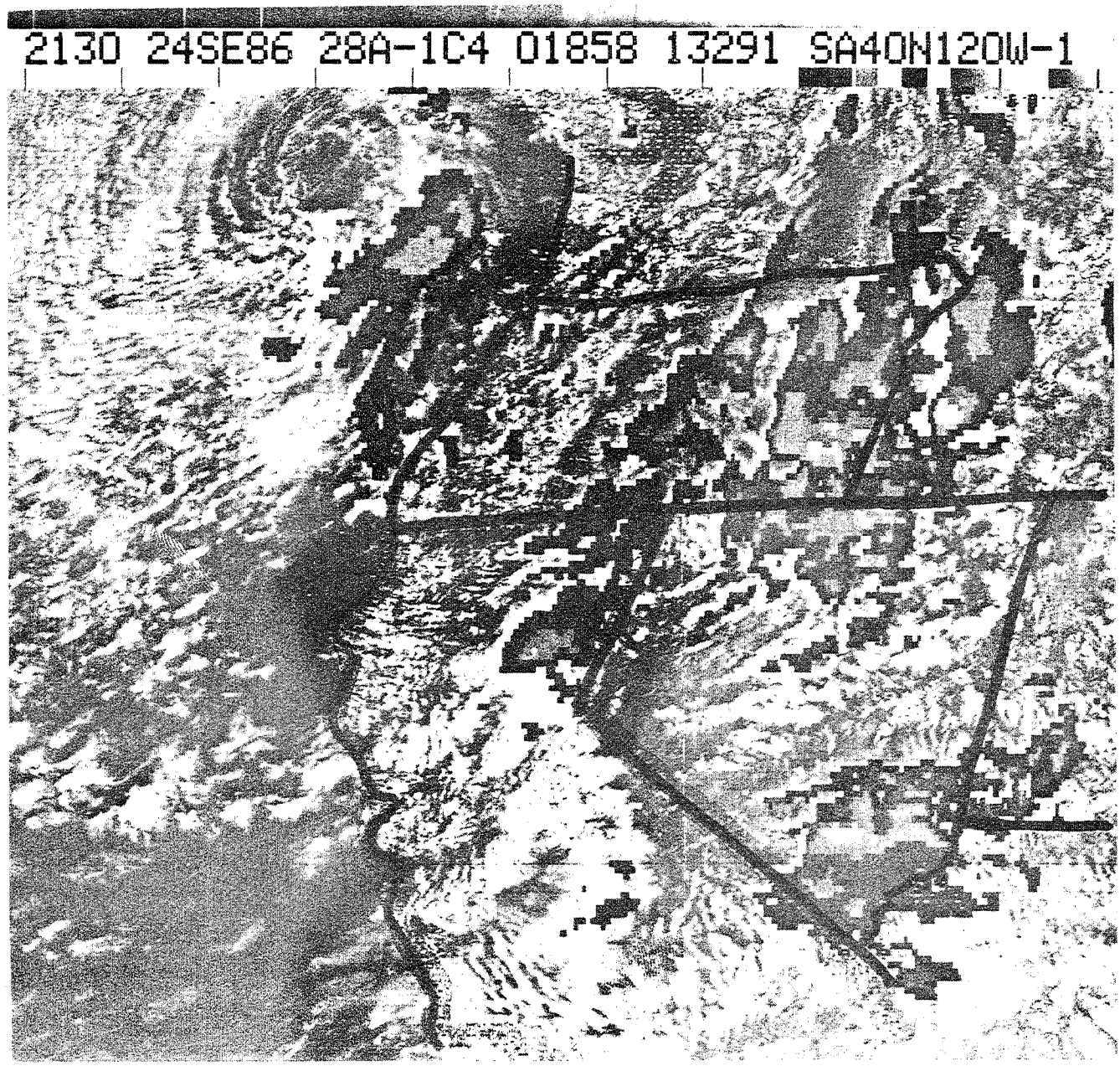

Figure 10d. Enhanced infrared satellite image for 2130 UTC (1330 LST) 24 September 1986.

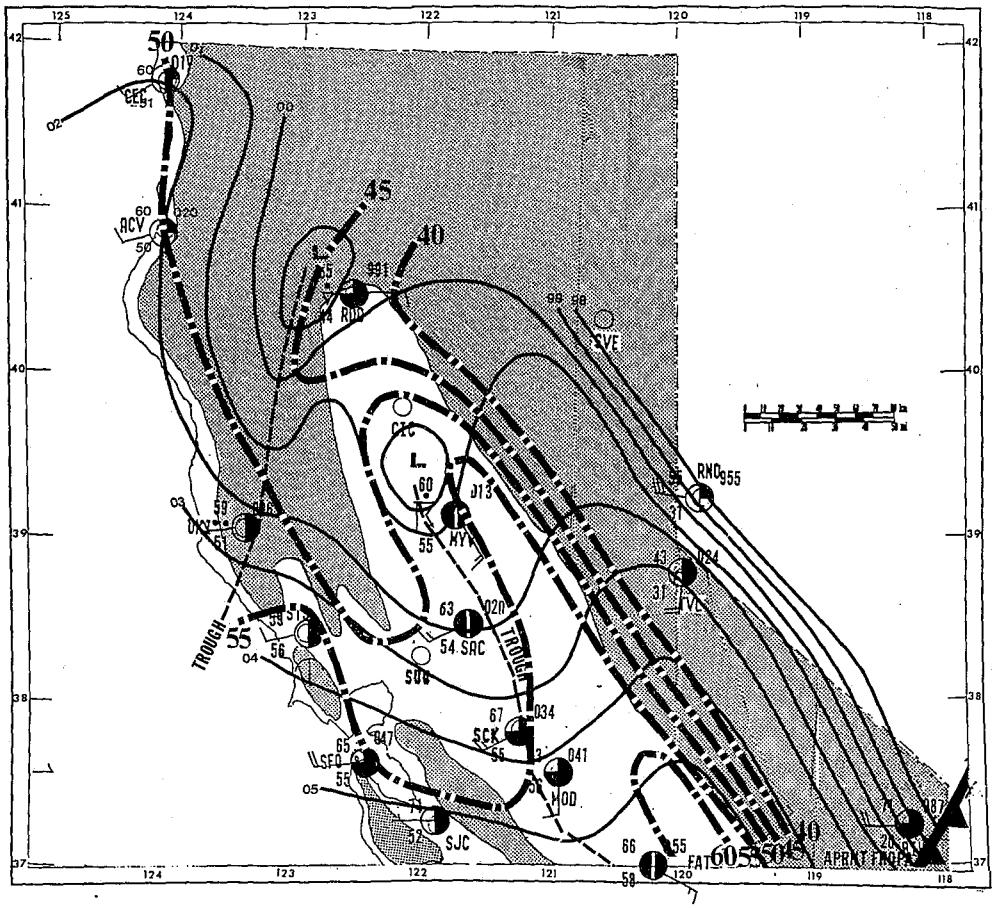

Figure 11a. As in Figure 8a, except for 2200 UTC (1400 LST).

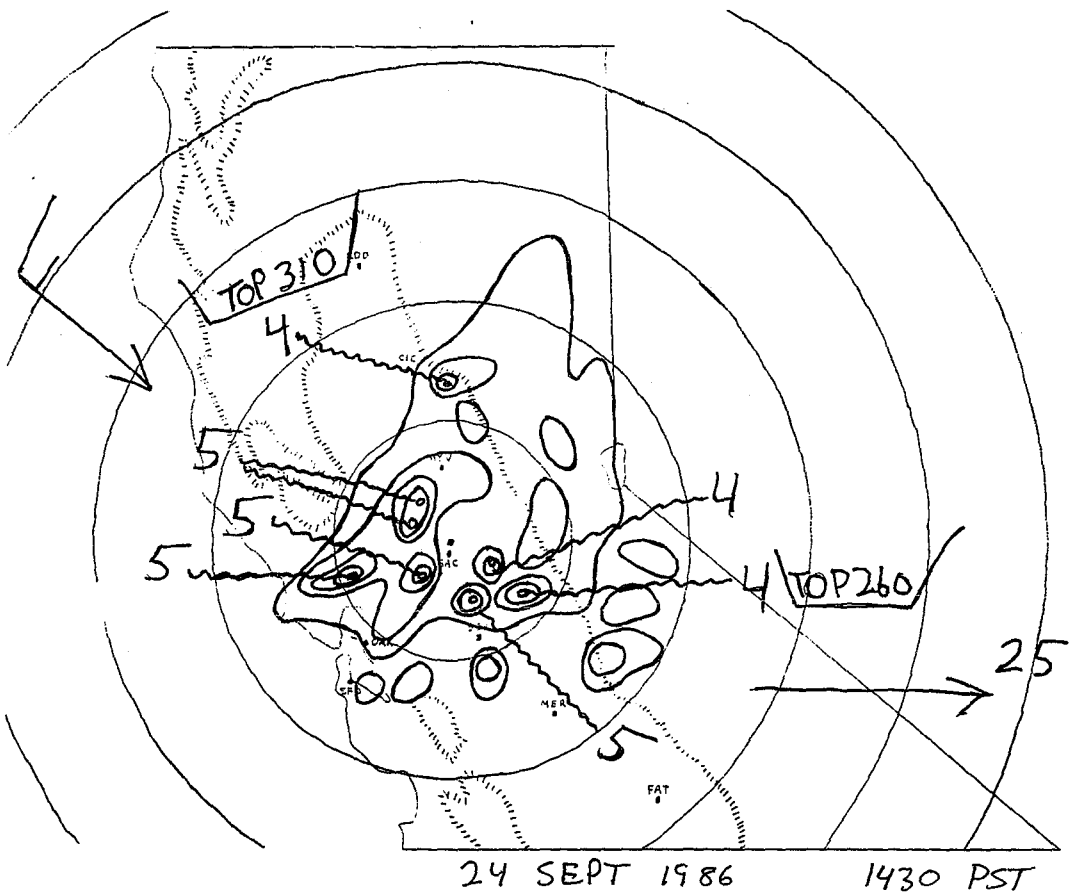

Figure 11b. As in Figure 8b, except for 2230 UTC (1430 LST).

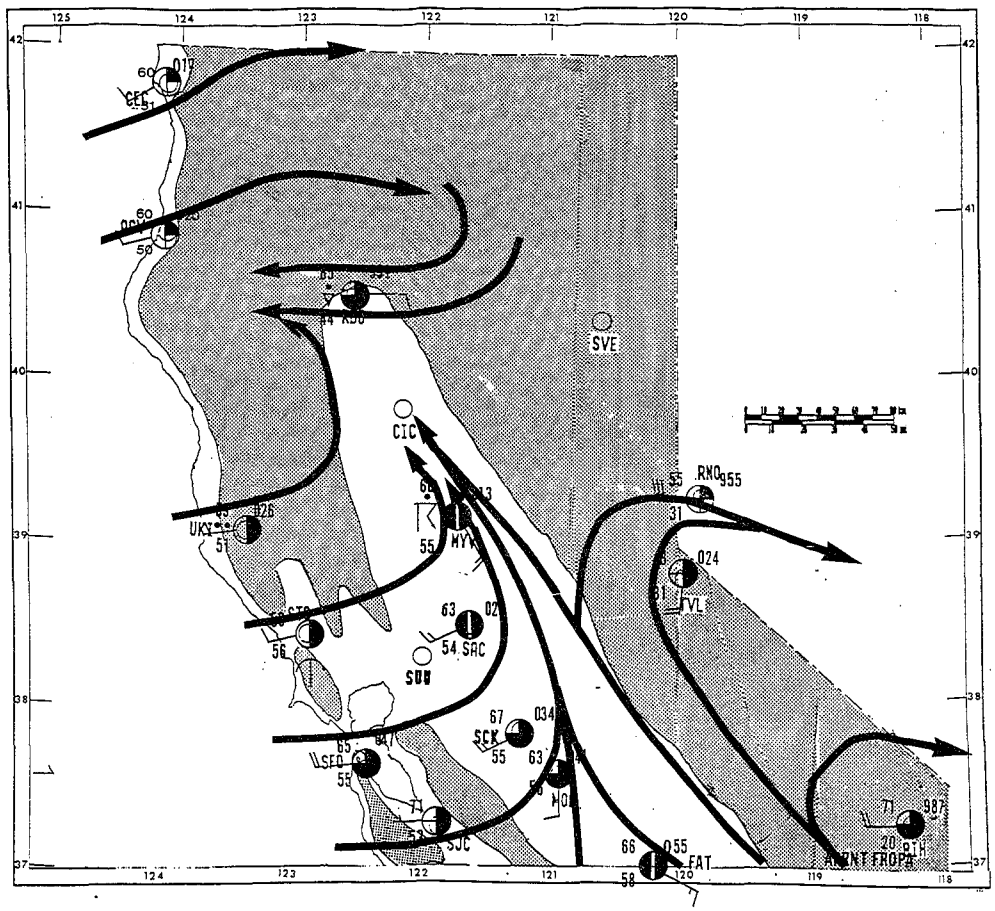

Figure 11c. As in Figure 8d, except for 2200 UTC (1400 LST).

Figure 11d. As in Figure 10d, except for 2230 UTC (1430 LST).

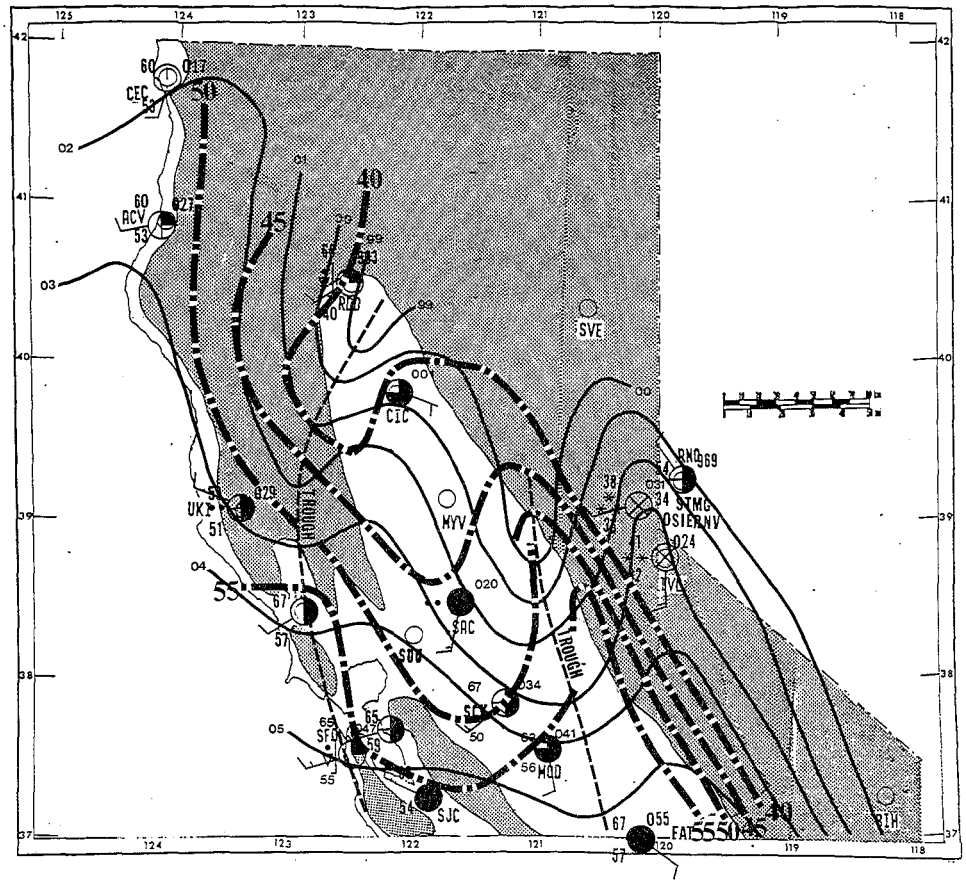

Figure 12a. As in Figure 8a, except for 2300 UTC (1500 LST).

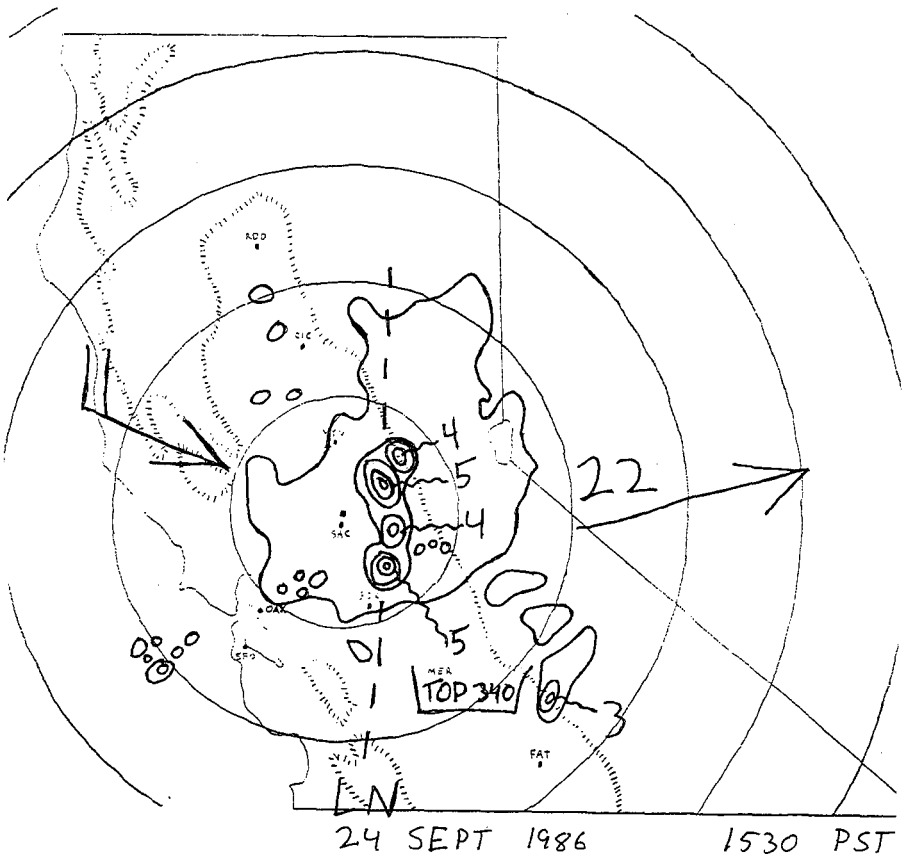

Figure 12b. As in Figure 8b, except for 2330 UTC (1530 LST).

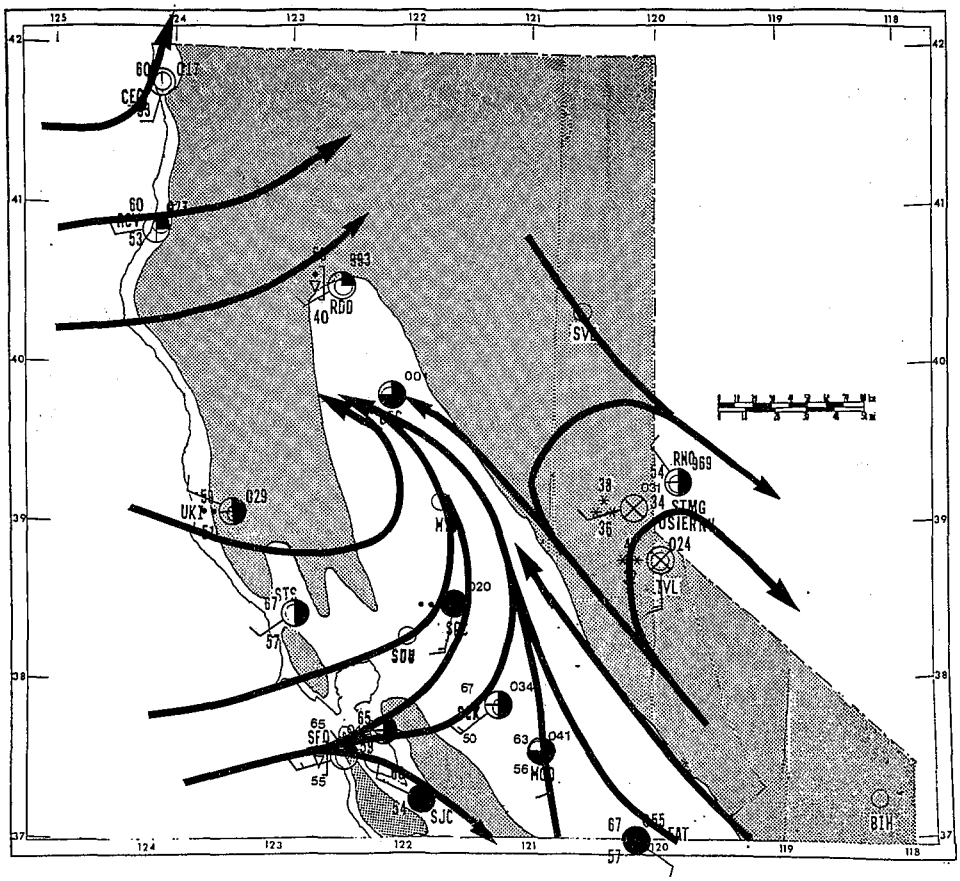

Figure 12c. As in Figure 8d, except for 2300 UTC (1500 LST).

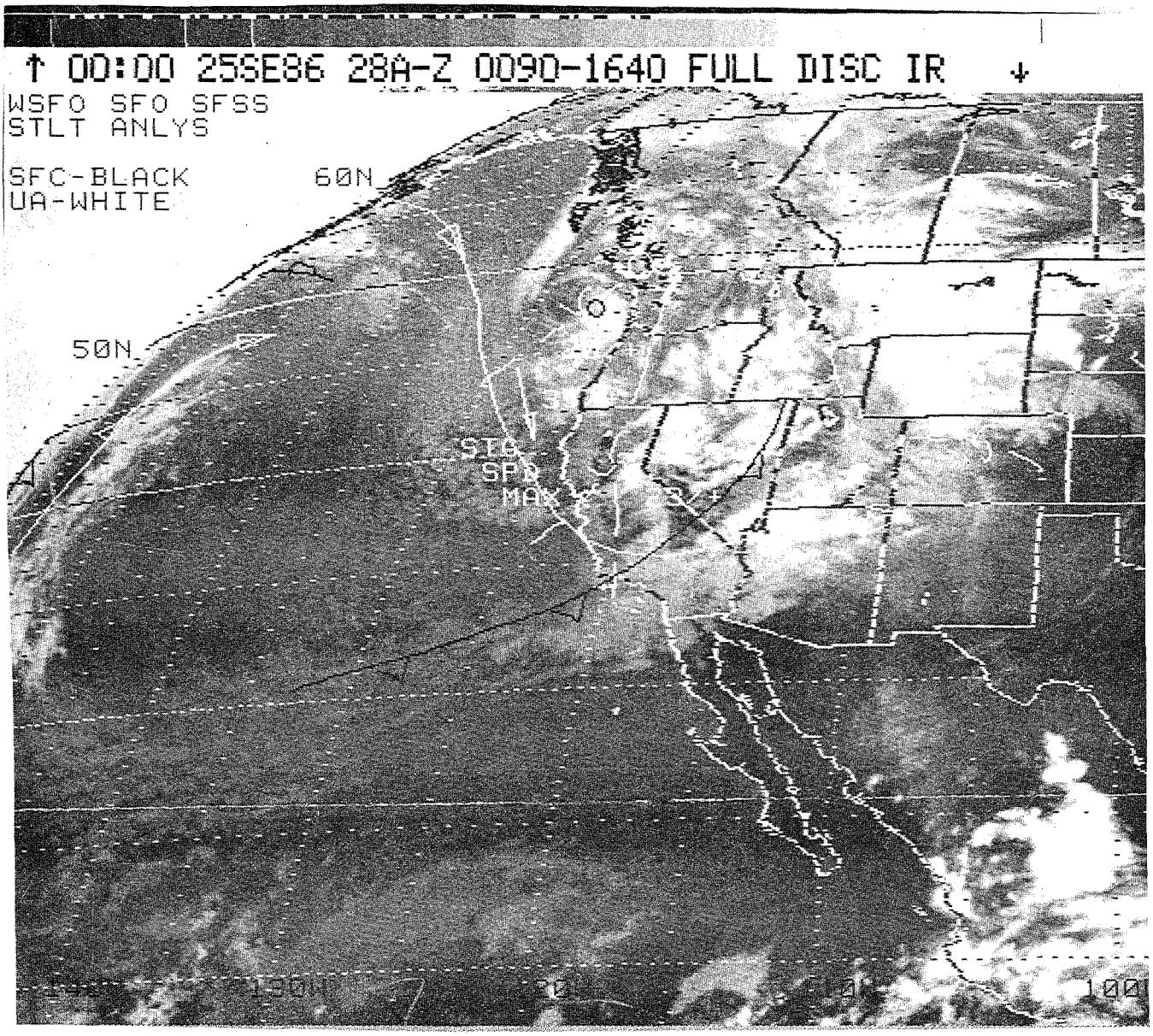

Figure 12d. As in Figure 7, except for 0000 UTC (1600 LST).

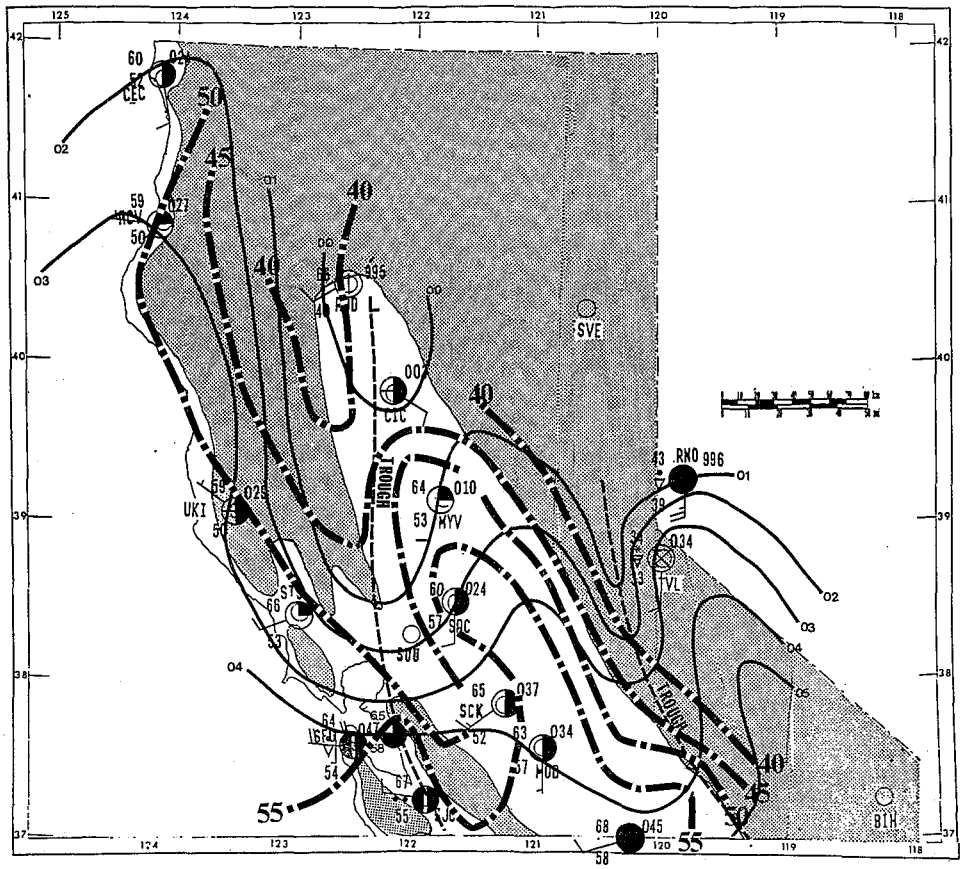

Figure 13a. As in Figure 8a, except for 0000 UTC (1600 LST).

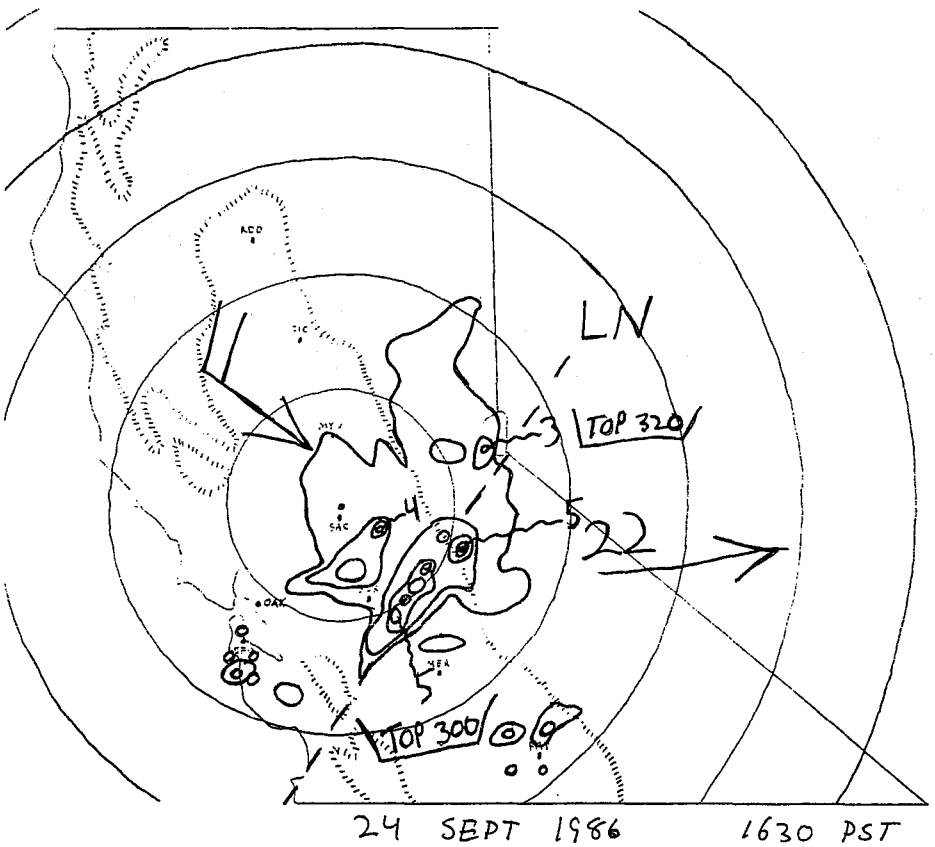

Figure 13b. As in Figure 8b, except for 0030 UTC (1630 LST).

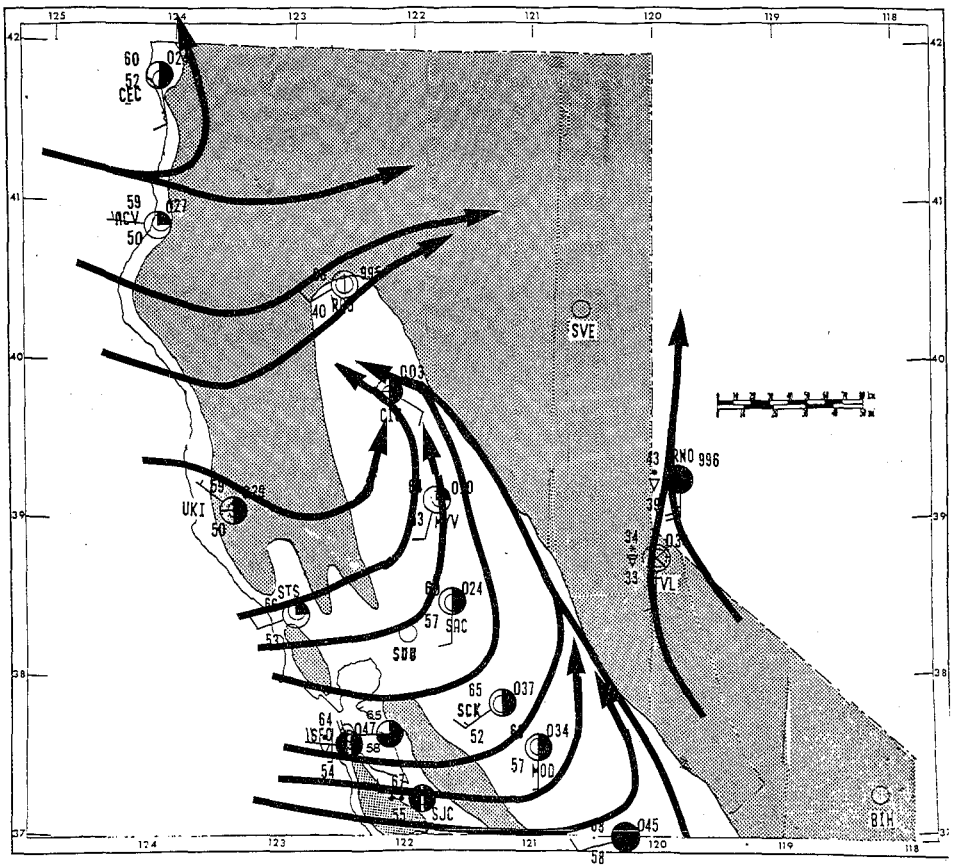

Figure 13c. As in Figure 8d, except for 0000 UTC (1600 LST).

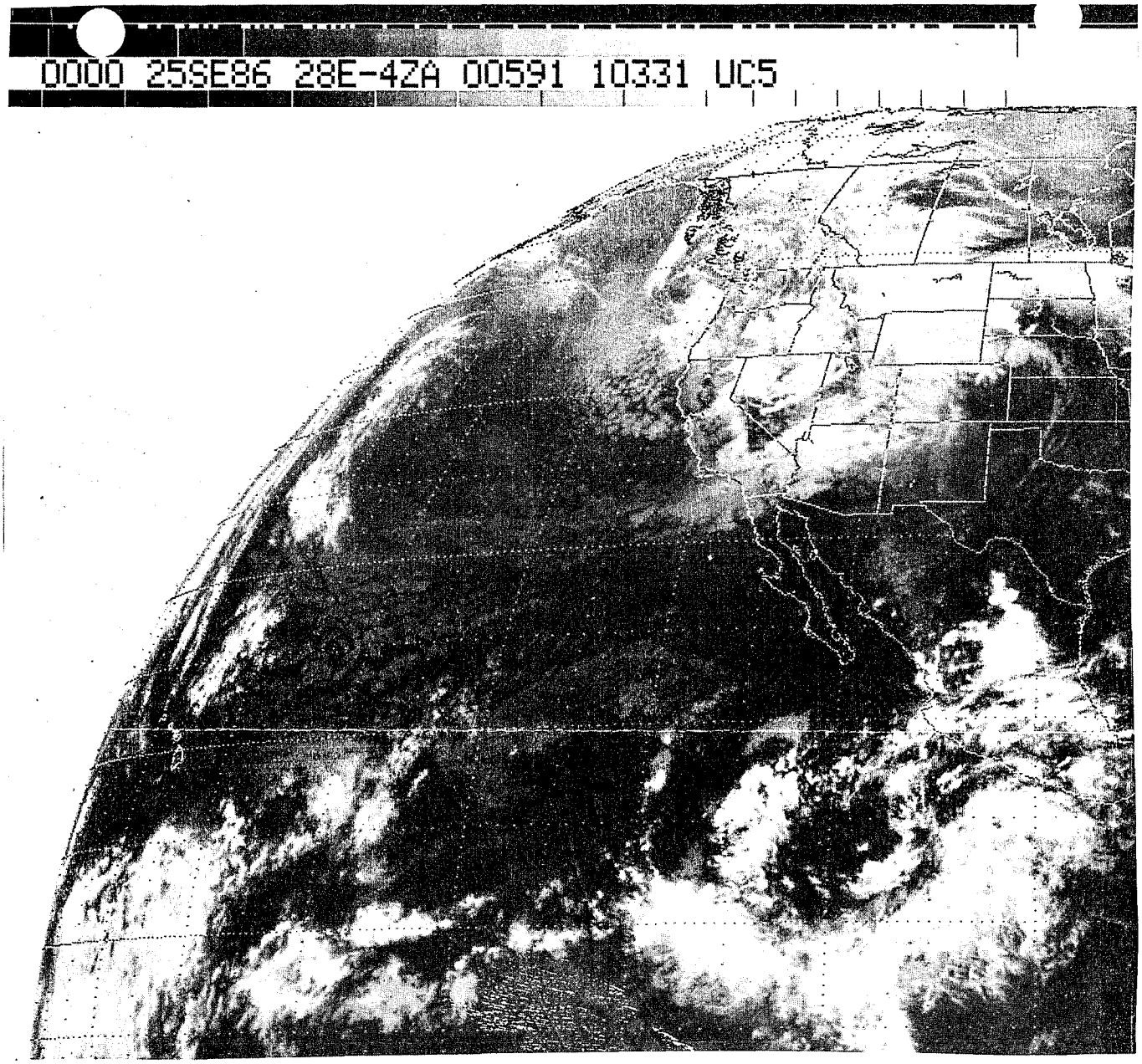

Figure 13d. As in Figure 8e, except for 0000 UTC (1600 LST).

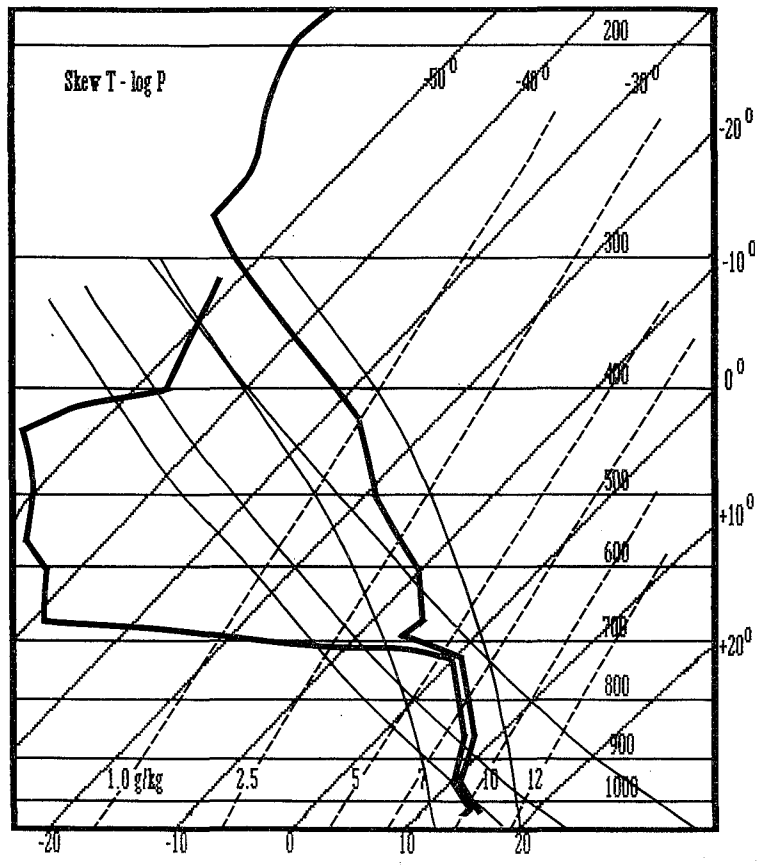

Figure 14. 1200 UTC (0400 LST) 24 September 1986 Oakland sounding plotted on schematic skew T-log P diagram.

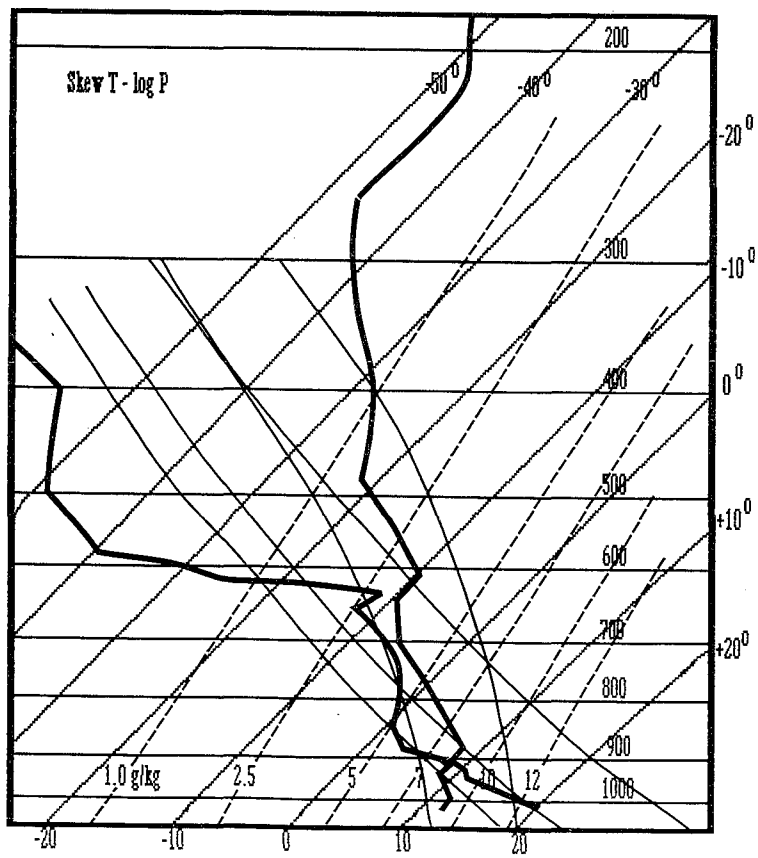

Figure 15. As in Figure 14, except for 0000 UTC 25 September 1986 (1600 LST 24 September 1986).

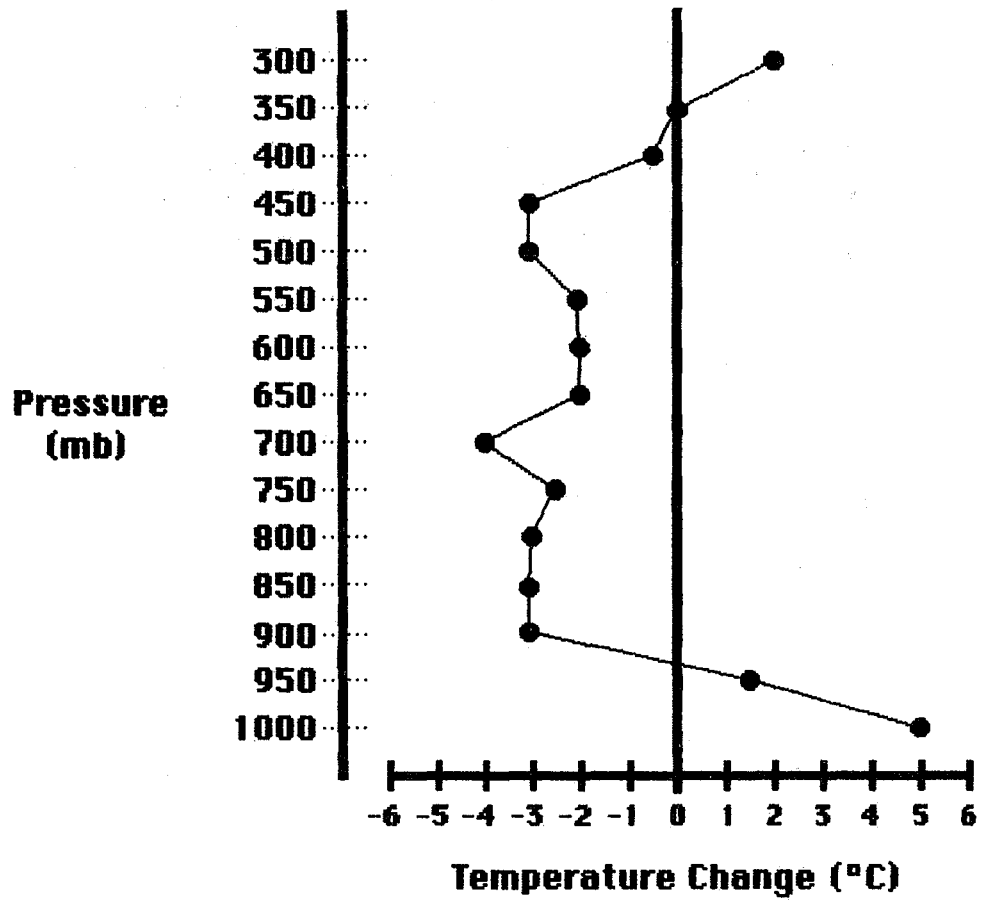

Figure 16. Layer temperature change at Oakland from 1200 UTC 24 September to 0000 UCT 25 September (0400 LST to 1600 LST 24 September) 1986.

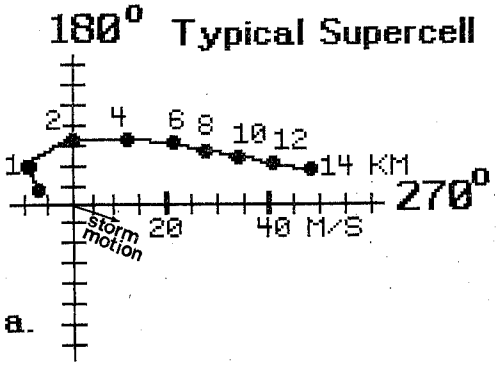

Figure 17a. Hodograph for typical hail producing supercell in Alberta (after Chisolm and Renick, 1972).

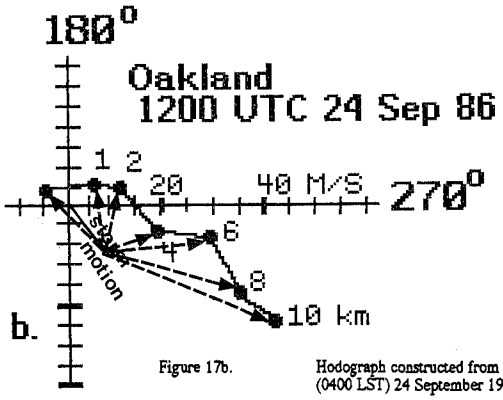

Figure 17b. Hodograph constructed from modified 1200 UTC (0400 LST) 24 September 1986 Oakland sounding.

Dashed arrows show storm relative flow (explained in text).

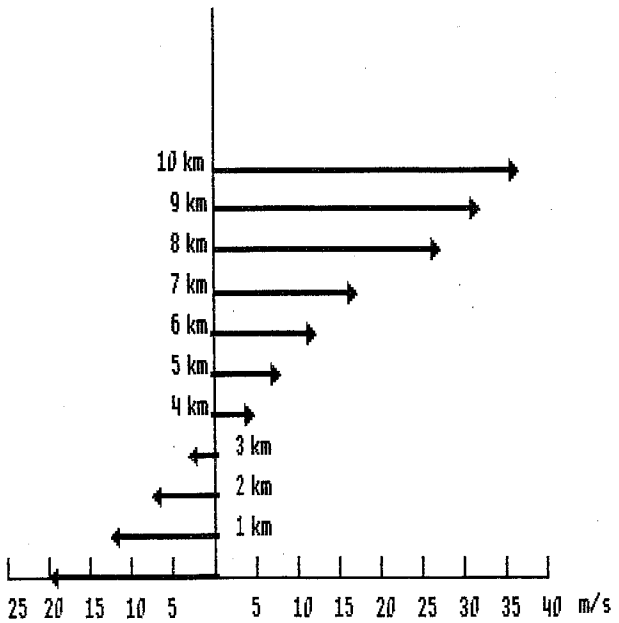

Figure 18. Schematic diagram showing flow relative to Redding storm.

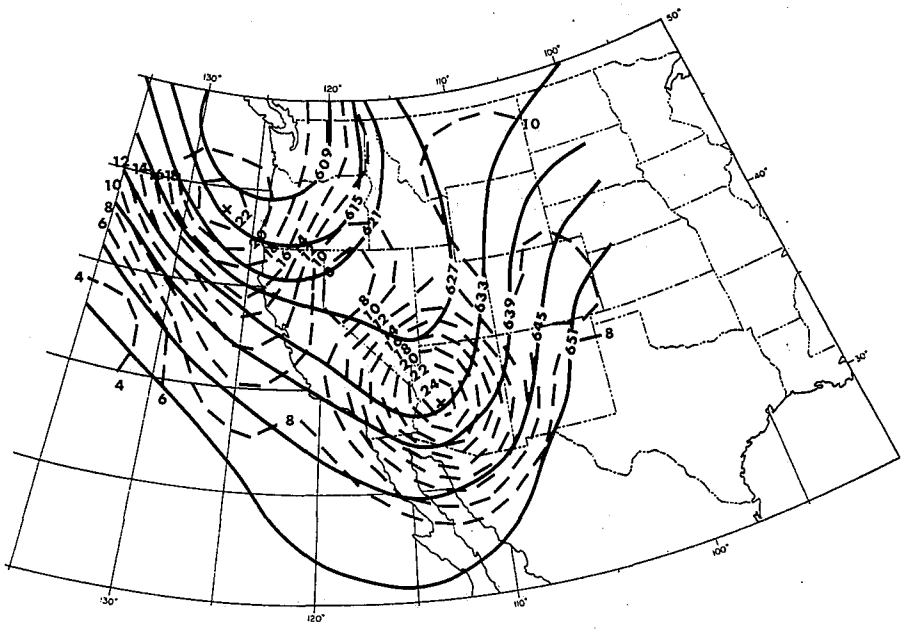

Figure 19. 700-300 mb thicknesses (solid, decameters) and 500 mb absolute vorticity (X 10^{-5}sec^{-1}) for 1200 UTC (0400 LST) 24 September 1986.

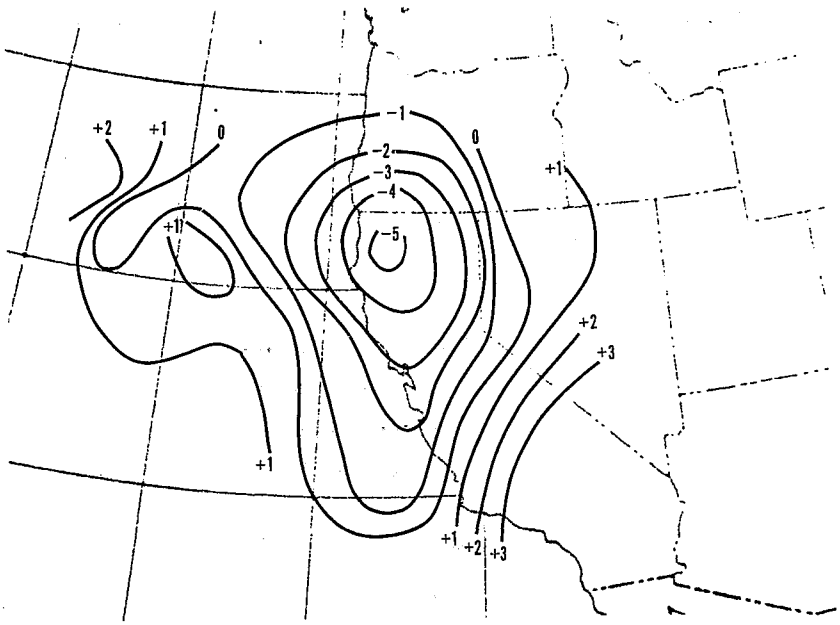

Figure 20. Contours showing quasi-geostrophically diagnosed field of omega (μb sec^{-1}) at 1200 UTC (0400 LST) 24 September 1986.

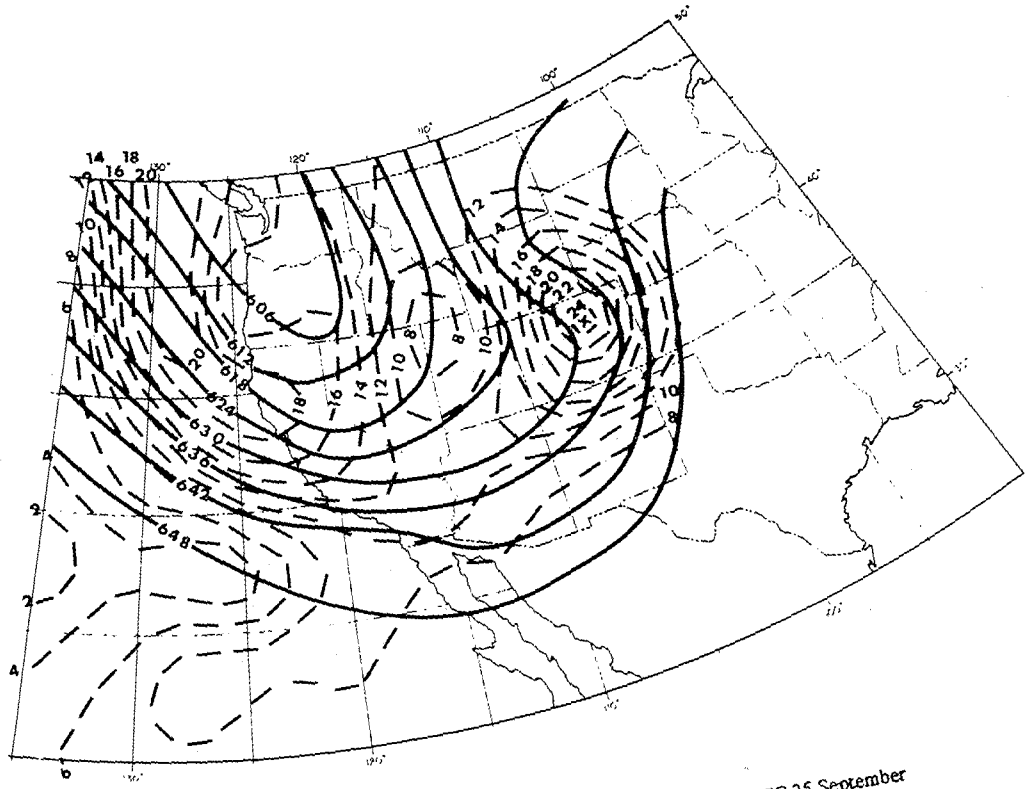

Figure 21. As in Figure 19, except for 0000 UTC 25 September (1600 LST 24 September) 1986.

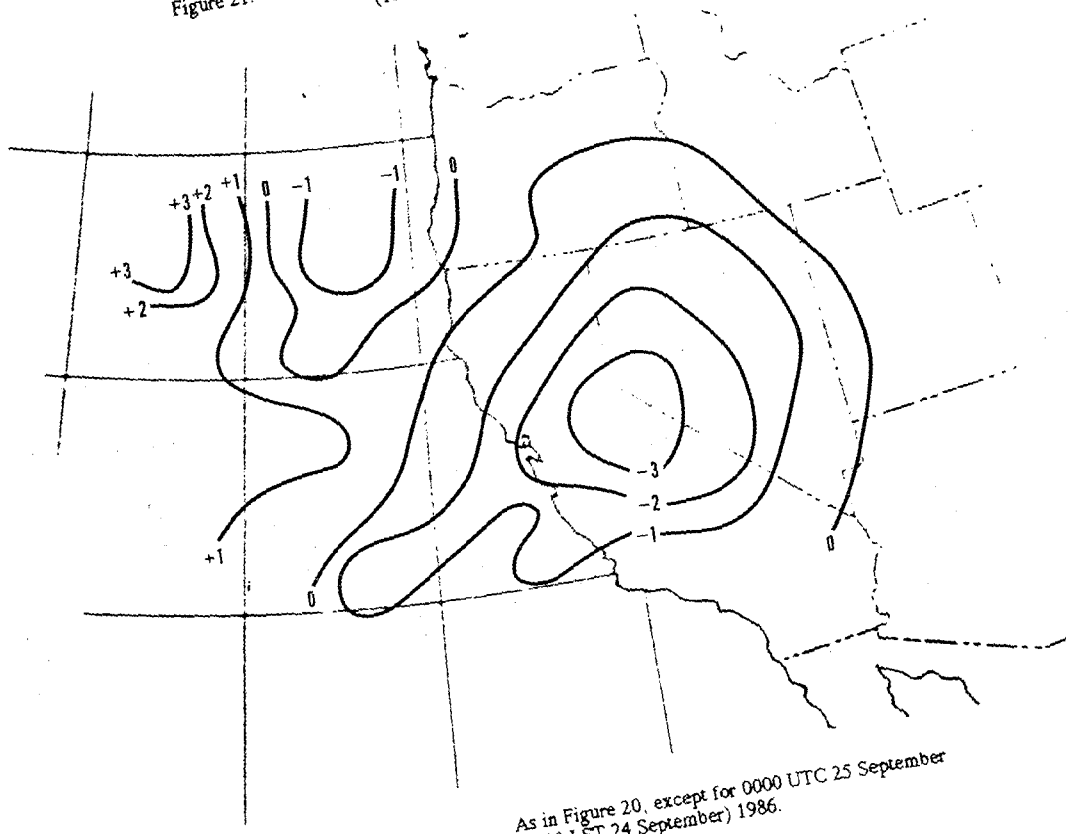

Figure 22. As in Figure 20, except for 0000 UTC 25 September (1600 LST 24 September) 1986.

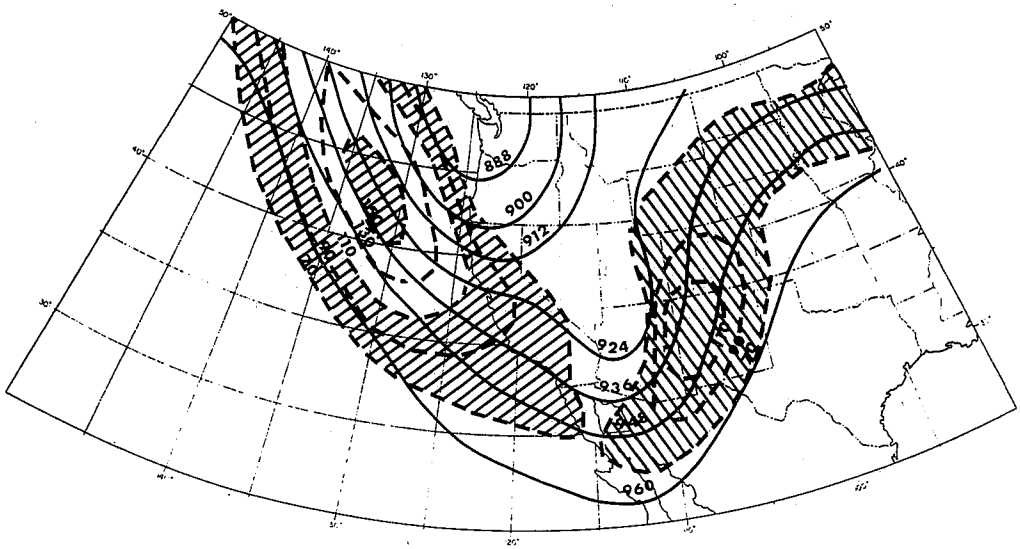

Figure 23. Facsimile of NMC 300 mb height (decameters) and isotach (knots) analyses for 1200 UTC (0400 LST) 24 September 1986.

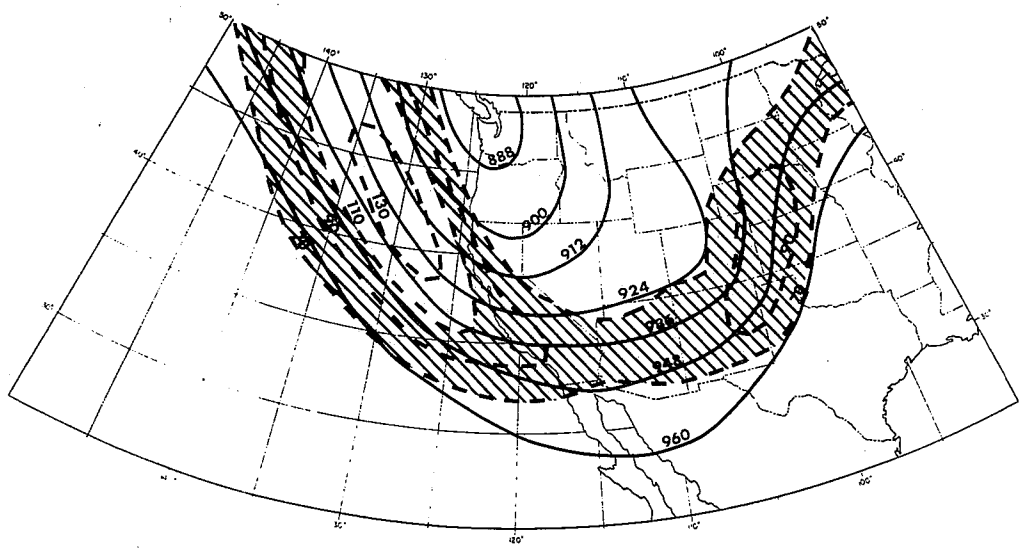

Figure 24. As in Figure 23, except for 0000 UTC 25 September (1600 LST 24 September) 1986.

140 Influence of Cloudiness on Summertime Temperatures in the Eastern Washington Fire Weather district. James Holcomb, April 1979. (PB298674/AS)
141 Comparison of LFM and MFM Precipitation Guidance for Nevada During Doreen. Christopher Hill, April 1979. (PB298613/AS)
142 The Usefulness of Data from Mountaintop Fire Lookout Stations in Determining Atmospheric Stability. Jonathan W. Corey, April 1979. (PB298899/AS)
143 The Depth of the Marine Layer at San Diego as Related to Subsequent Cool Season Precipitation Episodes in Arizona. Ira S. Brenner, May 1979. (PB298817/AS)
144 Arizona Cool Season Climatological Surface Wind and Pressure Gradient Study. Ira S. Brenner, May 1979. (PB298900/AS)
146 The BART Experiment. Morris S. Webb, October 1979. (PB80 155112)
147 Occurrence and Distribution of Flash Floods in the Western Region. Thomas L. Dietrich, December 1979. (PB80 160344)
149 Misinterpretations of Precipitation Probability Forecasts. Allan H. Murphy, Sarah Lichtenstein, Baruch Fischhoff, and Robert L. Winkler, February 1980. (PB80 174576)
150 Annual Data and Verification Tabulation - Eastern and Central North Pacific Tropical Storms and Hurricanes 1979. Emil B. Gunther and Staff, EPHC, April 1980. (PB80 220486)
151 NMC Model Performance in the Northeast Pacific. James E. Overland, PMEL-ERL, April 1980. (PB80 196033)
152 Climate of Salt Lake City, Utah. Wilbur E. Figgins, Third Revision January 1987. (PB87 157194/AS)
153 An Automatic Lightning Detection System in Northern California. James E. Rea and Chris E. Fontana, June 1980. (PB80 225592)
154 Regression Equation for the Peak Wind Gust 6 to 12 Hours in Advance at Great Falls During Strong Downslope Wind Storms. Michael J. Oard, July 1980. (PB91 108367)
155 A Raininess Index for the Arizona Monsoon. John H. Ten Harkel, July 1980. (PB81 106494)
156 The Effects of Terrain Distribution on Summer Thunderstorm Activity at Reno, Nevada. Christopher Dean Hill, July 1980. (PB81 102501)
157 An Operational Evaluation of the Scofield/Oliver Technique for Estimating Precipitation Rates from Satellite Imagery. Richard Ochoa, August 1980. (PB81 108227)
158 Hydrology Practicum. Thomas Dietrich, September 1980. (PB81 134033)
159 Tropical Cyclone Effects on California. Arnold Court, October 1980. (PB81 133779)
160 Eastern North Pacific Tropical Cyclone Occurrences During Intraseasonal Periods. Preston W. Leftwich and Gail M. Brown, February 1981. (PB81 205494)
161 Solar Radiation as a Sole Source of Energy for Photovoltaics in Las Vegas, Nevada, for July and December. Darryl Randerson, April 1981. (PB81 224503)
162 A Systems Approach to Real-Time Runoff Analysis with a Deterministic Rainfall-Runoff Model. Robert J.C. Burnash and R. Larry Ferral, April 1981. (PB81 224495)
163 A Comparison of Two Methods for Forecasting Thunderstorms at Luke Air Force Base, Arizona. LTC Keith R. Cooley, April 1981. (PB81 225393)
164 An Objective Aid for Forecasting Afternoon Relative Humidity Along the Washington Cascade East Slopes. Robert S. Robinson, April 1981. (PB81 23078)
165 Annual Data and Verification Tabulation, Eastern North Pacific Tropical Storms and Hurricanes 1980. Emil B. Gunther and Staff, May 1981. (PB82 230336)
166 Preliminary Estimates of Wind Power Potential at the Nevada Test Site. Howard G. Booth, June 1981. (PB82 127036)
167 ARAP User's Guide. Mark Mathewson, July 1981, Revised September 1981. (PB82 196783)
168 Forecasting the Onset of Coastal Gales Off Washington-Oregon. John R. Zimmerman and William D. Burton, August 1981. (PB82 127051)
169 A Statistical-Dynamical Model for Prediction of Tropical Cyclone Motion in the Eastern North Pacific Ocean. Preston W. Leftwich, Jr., October 1981. (PB82195298)
170 An Enhanced Plotter for Surface Airways Observations. Andrew J. Spry and Jeffrey L. Anderson, October 1981. (PB82 153883)
171 Verification of 72-Hour 500-MB Map-Type Predictions. R.F. Quiring, November 1981. (PB82 158098)
172 Forecasting Heavy Snow at Wenatchee, Washington. James W. Holcomb, December 1981. (PB82 177783)
173 Central San Joaquin Valley Type Maps. Thomas R. Crossan, December 1981. (PB82 196064)
174 ARAP Test Results. Mark A. Mathewson, December 1981. (PB82 198103)
176 Approximations to the Peak Surface Wind Gusts from Desert Thunderstorms. Darryl Randerson, June 1982. (PB82 253089)
177 Climate of Phoenix, Arizona. Robert J. Schmidli, April 1969 (Revised December 1986). (PB87 142063/AS)
178 Annual Data and Verification Tabulation, Eastern North Pacific Tropical Storms and Hurricanes 1982. E.B. Gunther, June 1983. (PB85 106078)
179 Stratified Maximum Temperature Relationships Between Sixteen Zone Stations in Arizona and Respective Key Stations. Ira S. Brenner, June 1983. (PB83 249904)
180 Standard Hydrologic Exchange Format (SHEF) Version I. Phillip A. Pasteries, Vernon C. Bissel, David G. Bennett, August 1983. (PB85 106052)
181 Quantitative and Spacial Distribution of Winter Precipitation along Utah's Wasatch Front. Lawrence B. Dunn, August 1983. (PB85 106912)
182 500 Millibar Sign Frequency Teleconnection Charts - Winter. Lawrence B. Dunn, December 1983. (PB85 106276)
183 500 Millibar Sign Frequency Teleconnection Charts - Spring. Lawrence B. Dunn, January 1984. (PB85 111367)
184 Collection and Use of Lightning Strike Data in the Western U.S. During Summer 1983. Glenn Rasch and Mark Mathewson, February 1984. (PB85 110534)
185 500 Millibar Sign Frequency Teleconnection Charts - Summer. Lawrence B. Dunn, March 1984. (PB85 111359)
186 Annual Data and Verification Tabulation eastern North Pacific Tropical Storms and Hurricanes 1983. E.B. Gunther, March 1984. (PB85 109635)
187 500 Millibar Sign Frequency Teleconnection Charts - Fall. Lawrence B. Dunn, May 1984. (PB85 110930)
188 The Use and Interpretation of Isentropic Analyses. Jeffrey L. Anderson, October 1984. (PB85 132694)
189 Annual Data & Verification Tabulation Eastern North Pacific Tropical Storms and Hurricanes 1984. E.B. Gunther and R.L. Cross, April 1985. (PB85 1878887AS)
190 Great Salt Lake Effect Snowfall: Some Notes and An Example. David M. Carpenter, October 1985. (PB86 119153/AS)
191 Large Scale Patterns Associated with Major Freeze Episodes in the Agricultural Southwest. Ronald S. Hamilton and Glenn R. Lussky, December 1985. (PB86 144474AS)
192 NWR Voice Synthesis Project: Phase I. Glen W. Sampson, January 1986. (PB86 145604/AS)
193 The MCC - An Overview and Case Study on Its Impact in the Western United States. Glenn R. Lussky, March 1986. (PB86 170651/AS)
194 Annual Data and Verification Tabulation Eastern North Pacific Tropical Storms and Hurricanes 1985. E.B. Gunther and R.L. Cross, March 1986. (PB86 170941/AS)
195 Radid Interpretation Guidelines. Roger G. Pappas, March 1986. (PB86 177680/AS)
196 A Mesoscale Convective Complex Type Storm over the Desert Southwest. Darryl Randerson, April 1986. (PB86 190998/AS)
197 The Effects of Eastern North Pacific Tropical Cyclones on the Southwestern United States. Walter Smith, August 1986. (PB87 106258AS)
198 Preliminary Lightning Climatology Studies for Idaho. Christopher D. Hill, Carl J. Gorski, and Michael C. Conger, April 1987. (PB87 180196/AS)
199 Heavy Rains and Flooding in Montana: A Case for Slantwise Convection. Glenn R. Lussky, April 1987. (PB87 185229/AS)
200 Annual Data and Verification Tabulation Eastern North Pacific Tropical Storms and Hurricanes 1986. Roger L. Cross and Kenneth B. Mielke, September 1987. (PB88 110895/AS)
201 An Inexpensive Solution for the Mass Distribution of Satellite Images. Glen W. Sampson and George Clark, September 1987. (PB88 114038/AS)
202 Annual Data and Verification Tabulation Eastern North Pacific Tropical Storms and Hurricanes 1987. Roger L. Cross and Kenneth B. Mielke, September 1988. (PB88 101935)

NOAA SCIENTIFIC AND TECHNICAL PUBLICATIONS

The National Oceanic and Atmospheric Administration was established as part of the Department of Commerce on October 3, 1970. The mission responsibilities of NOAA are to assess the socioeconomic impact of natural and technological changes in the environment and to monitor and predict the state of the solid Earth, the oceans and their living resources, the atmosphere, and the space environment of the Earth.

The major components of NOAA regularly produce various types of scientific and technical information in the following kinds of publications:

PROFESSIONAL PAPERS—Important definitive research results, major techniques, and special investigations.

CONTRACT AND GRANT REPORTS—Reports prepared by contractors or grantees under NOAA sponsorship.

ATLAS—Presentation of analyzed data generally in the form of maps showing distribution of rainfall, chemical and physical conditions of oceans and atmosphere, distribution of fishes and marine mammals, ionospheric conditions, etc.

TECHNICAL SERVICE PUBLICATIONS—Reports containing data, observations, instructions, etc. A partial listing includes data serials; prediction and outlook periodicals; technical manuals, training papers, planning reports, and information serials; and miscellaneous technical publications.

TECHNICAL REPORTS—Journal quality with extensive details, mathematical developments, or data listings.

TECHNICAL MEMORANDUMS—Reports of preliminary, partial, or negative research or technology results, interim instructions, and the like.

Information on availability of NOAA publications can be obtained from:

NATIONAL TECHNICAL INFORMATION SERVICE
U. S. DEPARTMENT OF COMMERCE
5285 PORT ROYAL ROAD
SPRINGFIELD, VA 22161